Resonant Ultrasound Spectroscopy of some oxide systems

A Thesis

submitted to
Indian Institute of Science Education and Research Pune
in partial fulfillment of the requirements for the
BS-MS Dual Degree Programme

by

Moirangthem Bicky Singh

Indian Institute of Science Education and Research Pune
Dr. Homi Bhabha Road,
Pashan, Pune 411008, INDIA.

August, 2021

Supervisor: Dr. Sunil Nair

Certificate

This is to certify that this dissertation entitled Resonant Ultrasound Spectroscopy of some oxide systems towards the partial fulfilment of the BS-MS dual degree programme at the Indian Institute of Science Education and Research, Pune represents study/work carried out by Moirangthem Bicky Singh at Indian Institute of Science Education and Research under the supervision of Dr. Sunil Nair, Associate Professor, Department of Physics , during the academic year 2020-2021.

Dr. Sunil Nair

Committee:

Dr. Sunil Nair

Dr. Surjeet Singh

This thesis is dedicated to my family

Declaration

I hereby declare that the matter embodied in the report entitled Resonant Ultrasound Spectroscopy of some oxide systems are the results of the work carried out by me at the Department of Physics, Indian Institute of Science Education and Research, Pune, under the supervision of Dr. Sunil Nair and the same has not been submitted elsewhere for any other degree.

Moirangthem Bicky Singh

Acknowledgments

First and foremost, I would like to thank my thesis supervisor, Dr. Sunil Nair, for his unparalleled support and guidance throughout this project. His immense knowledge and enthusiasm helped me steer the project in the right direction and fulfill the goal in a short period. Also, I am deeply indebted to him for always being there in my difficult times.

I would like to extend my sincere thanks to my labmates Dr.Arun, Dr.Avirup, Dr.Charu, Shruti, Sushmita, Haritha, Anna, and Murthy, for their encouragement and all the helpful discussions we had. Their insights and vast experiences had been invaluable to me in opening new ways to tackle the problem at hand. And they have imparted various priceless skillsets to broaden my expertise. I very much appreciate Shruti for clarifying many of my doubts and instilling inquisitiveness in me.

I would also like to thank my TAC, Dr. Surjeet Singh, for his guidance and for sharing his views on the project. I am extremely grateful to him for allowing me to use the Laue diffraction setup. I must also thank Dr. Shivprasad Patil for enabling me to characterize my transducers in his lab. Many thanks to Dibyata, who extended a great amount of assistance in the sample preparation and Laue diffraction; Surya for valuable ideas and his help in transducer characterization; Unmesh and Paul Freeman for their contribution in the analysis codes; and Kushal and Pranab for spending their precious time in answering my questions in LabView programming. Special thanks to Mr. Soman for fabricating my sample holder design and giving me helpful advice in designing too. Thanks also should go to all the people in the h-cross building for all their practical suggestions and assistance.

Last but not least, I would like to thank my family and friends for their support and care all through my studies. It would have not been possible without them.

Abstract

In the interminable quest for exciting properties in new materials, the measurements of elastic constants are of great importance. Among various techniques for measuring elastic constants, Resonance Ultrasound Spectroscopy (RUS) offers very high accuracy and efficiency. In this thesis work, we have built an RUS apparatus for room-temperature measurements on millimeter size samples. To this aim, we have designed the sample holder, fully automated the measurement setup, and calibrated the setup using KH_2PO_4 (KDP), a standard sample with known elastic constants. We have found that the measured resonance frequency spectra match well with the frequency spectra predicted from existing literature values of elastic constants at room temperature.In future, we aim to develop the setup further to perform temperature-dependent measurements extending down to liquid helium temperatures.

Contents

List of Figures

List of Tables

Chapter 1

Introduction

The most common ground behind measurements of elastic constants or elastic properties is to predict how a material deforms under the influence of stresses or forces. But, in the last few decades, people have found elastic properties measurements to be quite valuable for studying completely different but striking material properties in macroscopic and microscopic regimes. For instance, in condensed matter physics, they are usually exploited to probe phase transitions. Changes in temperature or pressure on a material invariably alter the shapes of curvatures of interatomic potentials in the material. On the other hand, elastic constants are the indirect measures of those curvatures (Fig. 1.1). So, any presence of structural, magnetic, or electric phase transitions associated with the temperature or pressure changes can be observed from "jumps" in the trends of the measured elastic constants of the material [3]. Besides, these constants are extremely helpful for the quantitative estimation of some thermodynamic quantities like specific heat capacity at constant volume (C_v), coefficient of thermal expansion, Debye temperature, and isothermal compressibility.

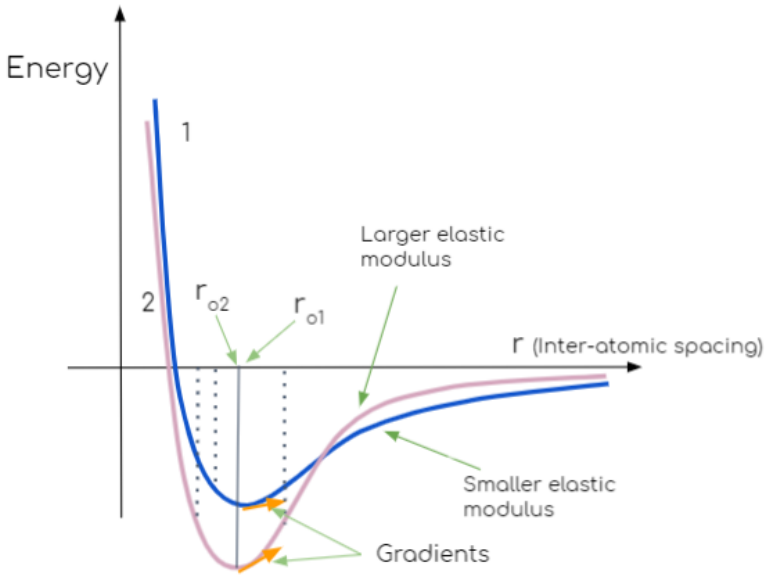

Figure 1.1: Interatomic potentials 1 and 2. The r_{o1} and r_{o2} are equilibrium spacings. The curvature (at r_{o1} or r_{o2}) and the spacing for each potential determine the elastic constants. (The greater the gradient or sharper the curvature, the larger the elastic constants are and vice-versa.)

Though theoretical (ab-initio calculations) and experimental (diffraction, scattering, stress-strain, ultrasonic, etc.) methods have been developed along the way to determine the elastic constants accurately, only the ultrasonic techniques are found to give the most accurate results at the moment [2][4]. There are two commonly used ultrasonic techniques viz- the Resonant ultrasound spectroscopy (RUS) based on natural resonance frequencies and the Pulse-echo approach based on sound velocity. Since the latter is labor-intensive for low symmetry solids and prone to error if there is a flaw or void in the solid [5], RUS is considered to be the best option.

Main parameters measured/computed	Representative methods	Approximate accuracies (typical)*
Theoretical/numerical	*Ab* initio calculation	Fair $(1-25\%)$
Stress-strain	Static, quasi-static, indentation	Fair $-$ good $(1-10\%)$
Speed of sound	Pulse-echo, continuous wave	Good - better $(<1\%)$
Frequencies	Resonance, RUS	Better - best $(0.1-1\%)$
Diffraction/Scattering	X-ray, neutron, Brillouin	Fair - good $(1-5\%)$)

$*$ Note: Accuracy of a method depends on elastic characteristic of the material, and note also that the accuracies (poor $\sim$ best) are for the whole category and subjective in nature.

Table 1.1: Elastic constants measuring methods along with their accuracies [2]

1.1 Resonant Ultrasound Spectroscopy

The Resonant Ultrasound Spectroscopy (RUS) is a technique where the mechanical resonances or normal modes frequencies of a solid are measured and used in computing the elastic constants. The mechanical resonance frequencies of a solid depend on size, symmetry, shape, density, and of course, elastic constants [3][6]. The first RUS-like method was introduced in the field of material sciences by LeCraw and Fraser in 1964 [7]. Later, Shereiber et. al and Demarest helped in improving the method by developing computational tools to solve for elastic constants [8]. However, with the advent of powerful personal computers in the late 20th century, Migliori, Visscher, and others have brought the technique to its finest form [9][6]. This technique has offered many advantages in the study of physical behaviors of materials like phase transitions, melting mechanisms, magnetism, superconductivity, etc.[10][11][12]. Also, unlike other techniques for elastic constant determination, this technique does not need relatively large samples and repeated independent measurements on lots of samples to get the complete set of elastic constants, and can be used in isotropic and anisotropic (even for low symmetry) materials easily.

Any RUS apparatus consists of two main parts- instrumentation and computation. In the instrumentation part, electronics are used to excite a mechanical vibration in a sample and detect its response. Subsequently, the computation part deals with the determination of elastic moduli from known parameters of the sample. With the availability of RUS analysis software and extremely fast computers, the complex computations involved in the technique can be done easily. In this thesis, we have designed a RUS set-up first, measure the resonance frequencies of standard material at room temperature, and then use an analysis code to extract elastic constants of the material. Once the viability is tested at room temperature, we anticipate extending the technique at low temperatures for studying temperature-dependent phase transitions in strongly correlated oxides.

1.2 Outline of Dissertation

Chapter 1 briefly mentions the importance of elastic constants measurement and why we choose RUS as a technique in this work.

In Chapter 2, the theoretical background of the RUS technique is summarized. The first section is dedicated to the linear elasticity theory as the study of elastic constants falls in the linear elastic regime. Then, the second section presents the elastic constants of anisotropic materials. This is followed by discussing how acoustic waves travel in a solid and are connected to the elastic constants. The next section is entirely focused on the RUS technique itself. Firstly, we talk about the calculation of the resonance frequencies from a given set of sample's physical parameters. Then, the most important part of the technique, "The inverse problem" is elaborated further. The inverse problem deals with the mathematical way to compute the elastic constants.

Chapter 3 explains the experimental methodologies for performing the RUS. It starts from the instrumentation and data acquisition methods that we have used. The instrumentation part is similar to most regular RUS setups. Next, we move to the sample holder design and assembling of the transducer. In a subsection, the calibrations of the transducers are included. This subsection is vital because if the transducers cannot give proper vibrations in a particular range of frequencies, our RUS setup will not work. Further, the reader will find information on how the sample preparation and characterization are done in RUS. Before ending the chapter, the procedure of performing a RUS scan is explained.

In Chapter 4, the results of our experiments are discussed. Most of the discussions are fixated on the reproducibility of the data, extractions of frequencies, and computing elastic constants.

In Chapter 5, the conclusion and scope of future work are described.

In Appendix, the sample holder construction details, data acquisition LabView program and analysis codes are included.

Chapter 2

Theoretical review of RUS

2.1 Linear elasticity theory

Elasticity is the ability of a material to regain its original shape and size when the applying forces which produce the deformation are removed. In the elasticity theory, the basic goal is to relate the deforming forces with the amount of deformation. To begin with, let us take an example of a 1D spring. Consider two points on the spring, one marked at x and another marked at $x + dx$, as shown in Fig. 2.1.

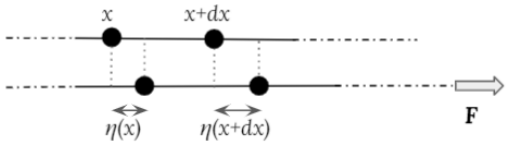

Figure 2.1: 1D spring before and after the force is applied.

When force F is applied, the points are displaced by an amount $\eta(x)$ and $\eta(x + dx)$. The strain (ϵ) is defined as the fractional amount of deformation, so,

$$\epsilon \equiv \frac{\eta(x + dx) - \eta(x)}{dx} = \frac{d\eta}{dx} \tag{2.1}$$

And, according to Hooke's law, $F = -kd\eta \propto \eta$ for the spring, where k is some constant. This can be further extended in the case of a 3D elastic body, where more degrees of freedom

are involved. The stresses (σ, forces per unit area) and strains (ϵ) for small deformations in a solid are related by (generalized Hooke's law):

$$\sigma_{ij} = \sum_{k=1,l=1}^{3} C_{ijkl}\epsilon_{kl} \tag{2.2}$$

where $i, j, k, l = \{x, y, z\}$ in Cartesian coordinates and C_{ijkl} are the elastic constants that form the elastic tensor. It is to be noted that the stresses and strains are turned into 2nd rank tensors here. In the stress notation, the first subscript tells the direction of the force, while the second refers to the direction of the normal to a surface. Similarly, in the strain notation, the first subscript refers to the direction of deformation while the second one indicates the rest length along a particular direction. In Fig. 2.2, to make things a bit clear, two types of strains are shown along with the corresponding stresses that caused them. Both the stress

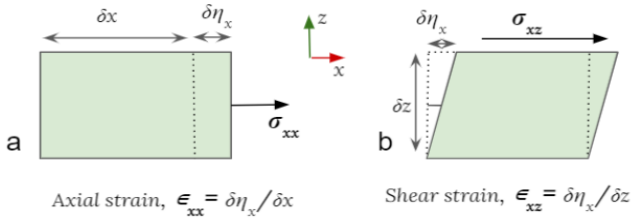

Figure 2.2: Two types of strains for a 3D elastic body

and strain tensors are symmetric in nature, meaning that $\sigma_{ij} = \sigma_{ji}$ and $\epsilon_{ij} = \epsilon_{ji}$. So, there exist only six independent components of stress and another six independent components of strain. Further, this forces the number of independent elastic constants or C_{ijkl} tensor components to 36. The elastic potential energy, which is the energy that gives the body to restore in its own shape, is quadratic in strains i.e., $U = \frac{1}{2}C_{ijkl}\epsilon_{ij}\epsilon_{kl}$. This allows us to swap ij and kl indices without changing the elastic potential energy U. Thus, the final number of independent C_{ijkl} reduces to 21, and the generalized Hooke's law takes the following matrix form after applying all the symmetry relations:

$$\begin{bmatrix} \sigma_{11} \\ \sigma_{22} \\ \sigma_{33} \\ \sigma_{23} \\ \sigma_{13} \\ \sigma_{12} \end{bmatrix} = \begin{bmatrix} C_{1111} & C_{1122} & C_{1133} & C_{1123} & C_{1113} & C_{1112} \\ & C_{2222} & C_{2233} & C_{2223} & C_{2213} & C_{2212} \\ & & C_{3333} & C_{3323} & C_{3313} & C_{3312} \\ & & & C_{2323} & C_{2313} & C_{2312} \\ & \textit{symmetric} & & & C_{1313} & C_{1312} \\ & & & & & C_{1212} \end{bmatrix} \begin{bmatrix} \epsilon_{11} \\ \epsilon_{22} \\ \epsilon_{33} \\ 2\epsilon_{23} \\ 2\epsilon_{13} \\ 2\epsilon_{12} \end{bmatrix}$$

It can be mentioned that the elastic tensor, C_{ijkl}, is a 4th rank tensor. Working with the four indices, again and again, is cumbersome. So, in most literature, people also use the Voigt convention where the four indices $ijkl$ are reduced to only two, i.e., ij by using the rules: $11 \rightarrow 1, 22 \rightarrow 2, 33 \rightarrow 3, 23 \rightarrow 4, 13 \rightarrow 5, and\ 12 \rightarrow 6$ [13]. For example, C_{1133} reduces to C_{13}, C_{1313} reduces to C_{55}, C_{1112} reduces to C_{16}, etc.

2.2 Crystal symmetries

The elastic properties of a material are also determined by the crystal symmetries of the material. In the case of an isotropic material, the elastic properties remain the same along any chosen direction. But, say, for a tetragonal crystal, the properties along all principal crystallographic axes will not be the same. Thus, symmetries are imposed on the elastic tensor by the crystal symmetries too. The table. 2.1 shows the relation between the independent elastic constants and crystal symmetries. Higher the symmetry, lower the number of the independent elastic constants.

Crystal class	No. of C_{ij}	Elastic constants
Triclinic	21	All possible combinations
Monoclinic	13	$C_{11}, C_{12}, C_{13}, C_{16}, C_{22}, C_{23}, C_{26}, C_{33}, C_{36}, C_{44}, C_{45}, C_{55}, C_{66}$
Orthorhombic	9	$C_{11}, C_{12}, C_{13}, C_{22}, C_{23}, C_{33}, C_{44}, C_{55}, C_{66}$
Trigonal	6 or 7	$C_{11}, C_{33}, C_{44}, C_{13}, C_{12}, C_{14}, C_{25}$
Tetragonal	6	$C_{11}, C_{33}, C_{44}, C_{13}, C_{12}, C_{66}$
Hexagonal	5	$C_{11}, C_{33}, C_{44}, C_{12}, C_{14}$
Cubic	3	C_{11}, C_{12}, C_{44}
Isotropic	2	C_{11}, C_{44}

Table 2.1: Independent elastic constants for all crystal symmetries [16]

The details for finding the independent constants depending on the crystal symmetries are found elsewhere in Phil Spoor's thesis [14] and the book *Ultrasonic Methods in Solid State Physics*[15].

2.3 Acoustic waves and elastic constants

Till now, the discussion is centered on static deformations only. For dynamic deformations, we need to know what elastic waves are. The time-dependent displacements in a small element of a solid can be related to the stress by using Newton's equation:

$$\frac{\partial \sigma_{ij}}{\partial x_j} = \rho \frac{\partial^2 \eta_i}{\partial t^2} \tag{2.3}$$

where ρ is the density of the solid. This equation can be further expanded as (using the Hooke's law and definition of strain):

$$C_{ijkl} \frac{\partial^2 \eta_k}{\partial x_j \partial x_l} = \rho \frac{\partial^2 \eta_i}{\partial t^2} \tag{2.4}$$

The solutions of the above equation represent the elastic waves. But, due to the tensor nature of the equation, the true forms of solutions and wave velocities are hard to imagine. However, the important point is the elastic waves can travel in different directions (longitudinally or transversely) even if the wave excitation is along a particular direction. In Pulse echo-technique, the fact that the elastic waves along different directions have different velocities is used. This technique, as mentioned earlier, can be used to determine the elastic constants by measuring the sound velocities (which are essentially the velocities of the elastic waves) across various crystallographic directions [16]. The sound velocity, v is related to the $Cij's$ and density ρ as - $v = \sqrt{\frac{\gamma(C_{ij})}{\rho}}$ where $\gamma(C_{ij})$ is some function of elastic constants. Even though the technique can give high accuracy in measuring elastic constants, this technique has some drawbacks. The two faces where the sound will be exciting and the echo will be reflected off should be perfectly parallel to one another. So, the technique needs a larger sample as many parallel faces need to be cut to measure the sound velocities in various directions. For low symmetry samples, it will even take a lot of time to cut the samples and perform the experiments. Also, any void or flaw inside the sample can scatter the sound waves hence, compromising the experiment. In RUS, a single measurement on a sample is needed to get the complete set of elastic constants of the sample.

2.4 The RUS Technique

2.4.1 Calculation of Resonance frequencies- The Forward problem

In RUS, the mechanical resonance frequencies of a solid with a well-defined shape are used to compute its elastic components. So, it is necessary to know how a relationship between elastic constants and resonance frequencies is developed. The problem of calculating the normal mode frequencies of a freely vibrating elastic solid was addressed in classical mechanics long ago. The common practice is to formulate the differential equations for the normal modes and find a time-harmonic solution after applying some boundary conditions. Due to the complexity of the differential equations, the analytical solutions exist only for isotropic spheres and isotropic rectangular parallelepipeds [14][17][18]. Thus, to approximate the resonance frequencies of various anisotropic solid shapes efficiently and connect them with elastic constants (moduli), Finite element Methods (FEM) and Lagrangian minimization methods are utilized. Even if FEM is the general approach, RUS mainly relies on Lagrangian minimization (Rayleigh-Ritz method) since RUS specifically deals with simple geometric objects, and the Lagrangian approach saves more computation time [5]. The Rayleigh-Ritz method is based on Hamilton's least action principle, where the Lagrangian of a system is stationary to small perturbations in eigenfunctions. Firstly, a freely vibrating solid, free of dissipation with density (ρ) is considered, and the Lagrangian of the system is written in terms of displacement field $\vec{\eta}(\vec{r})e^{-i\omega t}$ as-

$$L = \int_V (T - U)dV \tag{2.5}$$

where potential energy density

$$U = \frac{1}{2}C_{ijkl}\epsilon_{ij}\epsilon_{kl} = \frac{1}{2}C_{ijkl}\frac{\partial \eta_i}{\partial x_j}\frac{\partial \eta_k}{\partial x_l} \tag{2.6}$$

and kinetic energy density

$$T = \frac{1}{2}\rho\omega^2\eta_{\mathbf{i}} \cdot \eta_{\mathbf{i}} \tag{2.7}$$

for normal mode with angular frequency ω, which comes from the harmonic time dependence. Then, the Rayleigh-Ritz method approximates the displacement field around an equilibrium point $\vec{r}$ as an expansion of known basis functions set with unknown coefficients: $\vec{\eta}(\vec{r}) \approx$

$\sum_{i=1}^{3}\sum_{\nu=1}^{N}\alpha_{\nu,i}\phi_\nu(\vec{r})\hat{\mathrm{e}}_i$ where $\hat{\mathrm{e}}_i$ is a unit vector in Cartesian coordinates and N is the number of basis functions ϕ_ν. The expansion can be contracted for simplicity as

$$\vec{\eta}(\vec{r}) \approx \sum_{m=1}^{3N} \alpha_m \phi_m \hat{\mathrm{e}}(m), \quad \phi_m \in \phi_\nu \tag{2.8}$$

Substituting this expression for displacement field in L, we have,

$$L = U - T \approx \sum_{m,n} \alpha_m \alpha_n \Gamma_{mn} - \omega^2 \sum_{m,n} \alpha_m \alpha_n E_{mn} \tag{2.9}$$

where

$$\Gamma_{mn} = \int_V C_{i_m j k_n l} \frac{\partial \phi_m}{\partial x_j} \frac{\partial \phi_n}{\partial x_l} dV, \quad E_{mn} = \int_V \rho \phi_m \phi_n \delta_{i_m k_n} dV$$

Furthermore, L is compacted in matrix form as $L \approx \boldsymbol{\alpha}^{\mathbf{T}} (\boldsymbol{\Gamma}\boldsymbol{\alpha} - \omega^2 \mathbf{E}\boldsymbol{\alpha})$. By applying Hamilton's principle $\partial L/\partial \alpha_m = 0$, we get,

$$\boldsymbol{\Gamma}\boldsymbol{\alpha} - \omega^2 \mathbf{E}\boldsymbol{\alpha} = 0 \tag{2.10}$$

an eigenvalue problem. Standard techniques (analytical or numerical) can be used to solve such eigenvalue problems to get the natural resonance frequencies and eigenvectors (the expansion coefficients). So, if the mass density, sample dimensions, and elastic constants of a solid object are given, by following the above approach, which is usually referred to as the Forward problem, all normal modes can be determined.

The success of solving the above eigenvalue problem depends on what kinds of basis functions are chosen. There are three main criteria that have to be considered in choosing the basis: (a) The basis functions should be able to approximate the boundary conditions. Here, we consider a freely vibrating solid, which means the sample displacements are free at boundaries. So, the chosen basis functions should not have constraints on the displacements at boundaries too. (b) To find the elements of $\mathbf{E}$ and $\boldsymbol{\Gamma}$ matrices, the integrals of basis functions and their derivatives need to be performed analytically. Also, if we want to increase the accuracy in approximating the normal mode frequencies, the number of basis functions has to be increased, meaning that our eigenvalue problem will have much bigger matrices to deal with. Therefore, we should choose relatively simpler basis functions to make the above works easier. (c) Lastly, the basis functions should form a complete set because any linear

combinations of the functions should be able to approximate any possible displacements of the vibrating solid.

Basis sets of orthogonal trigonometric functions, Legendre polynomials, etc., have been tried, but they are limited only to a few geometries as the integrals are hard to solve [19][8][20]. Although, the most successful one is the Visscher basis set since the set offers more flexibility in the geometries of the solids. Besides, the integrals of $\mathbf{E}$ and $\mathbf{\Gamma}$ become similar, so one can write only a simple function to compute the integrals [21]. The Visscher basis consists of simple powers of cartesian coordinates $x^l y^m z^n$, where (l, m, n) are a set of positive integers which have to satisfy $N_o \geq l + m + n$, N_o is the maximum power. N_o is commonly set between 10 to 12 to get good accuracy.

2.4.2 Estimation of elastic constants - The Inverse problem

Now, one can ask what about going backward and determining the elastic constants from a set of experimentally measured resonance frequencies of the same solid object. Though inversion of the forward calculation is not possible mathematically [3][22], there is an interesting way to find the constants, which makes RUS a complete tool. The way, commonly known as the Inverse Problem, involves the forward calculation and a nonlinear fitting. With the available dimensions, density, measured resonance frequencies, and estimated C_{ijkl}'s, the forward computations are performed initially. Then, output frequencies are compared with measured frequencies iteratively and the parameters are adjusted in each step till certain tolerable levels are reached through a nonlinear least-squares fitting. The nonlinear fitting employs an algorithm like Lavenberg Marquardt (LM) [16] or a conjugate gradient method to minimize the non-linear error functional $G(x)$, defined as a sum of weighted squares of the difference between calculated and measured frequencies.

$$G(x) = \sum_{i=1}^{M} w_i \left[f_i^{(calc)}(x) - f_i^{(obsv)}(x) \right]^2$$

where w_i's, weight values are generally set as 1. Thus, the elastic constants can be deconvoluted from experimentally measured mechanical resonance frequencies.

For our analysis, python codes developed at Physical Acoustic Laboratory, University of New Zealand, to perform both forward and inverse calculations have been used. Both the

code and the manual are found on Github [23], or one can get a glimpse of how the code works in Zadler et.al. paper [24].

Chapter 3

Experimental methods

For resonance frequency measurement in RUS, a sample cut in the shape of rectangular parallelepiped (RPR) or sphere or cylinder is kept in between two piezoelectric or ferroelectric transducers. Then, one of the transducers is be driven with a swept sinusoidal voltage signal to excite mechanical vibrations (i.e., to induce changing stress fields, which is due to the transducer's compressional or shear mode) to the sample, while the other acts as a receiver of the sample's vibrational (strain) response. When the drive frequency matches the natural frequency of the sample, it vibrates strongly depending on the resonance quality factor ($Q = f_o/\Delta f$), which in turn generates a corresponding ac response across the receiving transducer. This is the brief idea behind the experimental measurement of resonance frequencies. Our goal here is to realize this idea by designing a complete RUS setup in the lab.

In this chapter, the experimental methodologies followed in developing our RUS setup for room temperature measurements are outlined. In addition, the techniques used in the sample preparation and performing a good RUS scan have been elucidated.

3.1 Instrumentation and data acquisition

In our RUS set-up, a function generator (Tektronix AFG 1022) that can give up to 25 MHz/ 10Vpp (peak to peak) sinusoidal voltage signal is used to drive a $LiNbO_3$ piezoelectric transducer. And a Lock In-Amplifier (LIA), SRS SR844 RF, is employed for detecting the sample response through a second $LiNbO_3$ transducer. RF coax cables with good shielding are used in all connections to avoid unwanted EM noise pick-ups and RF interferences. In the case of long coaxial cable connections, it is suggested to use a preamplifier to help in amplifying weak output signals before giving output directly to Lock-In Amplifier [5]. But, for our room temperature measurements, we do not feel the need for a preamplifier. Lastly, a LabView program has been developed to control these instruments and acquire data through USB and GPIB cables.

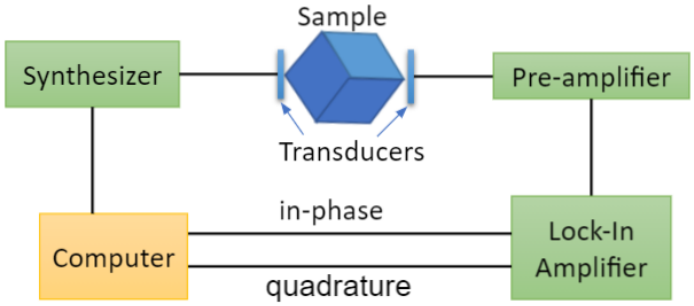

Figure 3.1: Block diagram of RUS

3.1.1 Phase-sensitive detection

Lock-In Amplifiers are commonly designed to detect and measure very small ac signals obscured in big noise sources. Even when the signal is thousands of times smaller than the noise sources, accurate measurements can still be made using them. They use a technique called Phase Sensitive Detection (PSD) to single out the component of the signal at a specific reference frequency and phase. The advantage of this technique is that all noise signals at frequencies other than the reference are rejected. For our experiments, a channel output from the function generator is fed to the LIA SR844 for locking its internal oscillator to a reference frequency, while another channel output, set at the same frequency that of reference, is used to excite the experiment. Then, the signal coming from the experiment is given to the SR844 signal input. Hence, SR844 detects only the right response at our desired reference frequency.

A short summary of Phase sensitive detection (PSD) technique is summarised in the following lines. Let us assume the reference signal as $V_r \sin(\omega_R t + \theta_r)$ and the sample response from the experiment as $V_i \sin(\omega_r t + \theta_i)$. Inside the LIA, a mixer multiplies the reference and response signals and generates the product of them as-

$$\begin{aligned} V_{mixture} &= V_r \sin(\omega_r t + \theta_r)\, V_i \sin(\omega_r t + \theta_i) \\ &= \frac{1}{2} V_r V_i \cos(\theta_r - \theta_i) + \frac{1}{2} V_r V_i \sin(2\omega_r t + \theta_r + \theta_i) \end{aligned} \tag{3.1}$$

The first term in the above output is a DC voltage because we give the inputs to the mixer at the exact same frequency. On the other hand, the second term is at AC with frequency $2\omega_r$ i.e., twice the reference frequency. So, this ac component is removed by passing through a low pass filter. After passing through the filter, the final output is

$$V_{mixture+filter} = \frac{1}{2} V_r V_i \cos(\theta_r - \theta_i) \tag{3.2}$$

where there is the cosine of the phase difference of the reference and the response inputs. Thus, the term Phase Sensitive Detection comes.

In the case of our SR844, there are two mixers, where one of the mixers takes a reference input with 90-degree out-of-phase. These two mixers help in the simultaneous determination of the amplitude and phase of the sample response. Further, the in-phase and quadrature components can also be computed once the values of the amplitude and phase of the signal input are determined.

3.1.2 Automation and Interfacing through LabView

Running a full scan in RUS involves incrementing the frequency in steps and measuring the sample response at each frequency. It will be tedious to do these jobs manually. So, a LabView program is developed to automate the instruments and to acquire data at the same time. Both GPIB and USB interfaces (installed on a personal computer) are used to communicate with instruments. It takes 3 seconds to take a reading, and the data are saved in .txt formats for future analysis.

To configure the instruments (both Function generator and LIA) comfortably, the instrumental drivers available on NI (National Instruments) websites are used in developing the program. The block diagram of the program is included in the appendix.

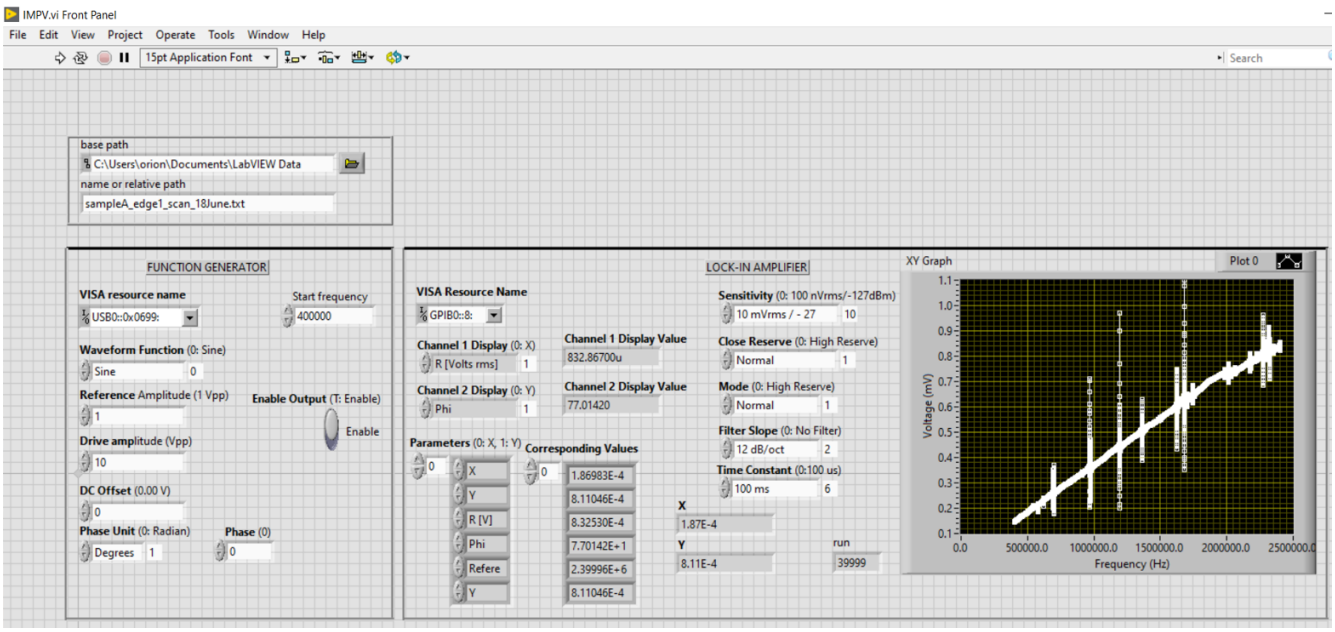

Figure 3.2: A snippet of LabView program (front face) for the automation and data acquisition. The resonance peaks can be observed on the Graph panel made on the right side.

3.2 Sample holder and transducers

Over the years, various RUS sample holder designs for extreme temperature measurements have been reported in the literature [5][4][22][3][Migliori et al. modern, High-temperature thesis, G. Li, Balkirev]. Most of them use either ferroelectric or piezoelectric transducers depending on the desired temperature ranges of operation. Sometimes, buffer rods in contact with the transducers are also used in the case of high-temperature measurements. But, for performing RUS on thin films and fragile samples, Gladden and Phil Spoor theses have nicely documented a special cell design based on PVDF films [16][14]. If in case required for only room temperature studies, RUS setups are also now commercially available from Dynamic Resonance Systems (DRS) and Quasar Inc [25][26]. However, to fulfill our goal, a RUS sample holder that can be used at low temperatures is independently designed. Two Z-cut $LiNbO_3$ piezoelectrics are also used as ultrasonic transducers. The following subsections narrate the descriptions of the sample holder design and transducer assembly.

3.2.1 Sample holder design

The structure of the sample holder mainly consists of two copper flanges, two hollow brass rods, and four brass supports, as shown in figure 3.3(a). Each of the two copper flanges holds one hollow brass rod at the center. The gap between the rods is adjustable by screwing the rods in and out. And, the brass supports hold both flanges at a fixed distance with the help of small hexagonal screws. In this sample holder, a sample as big as 5mm can be fitted easily.

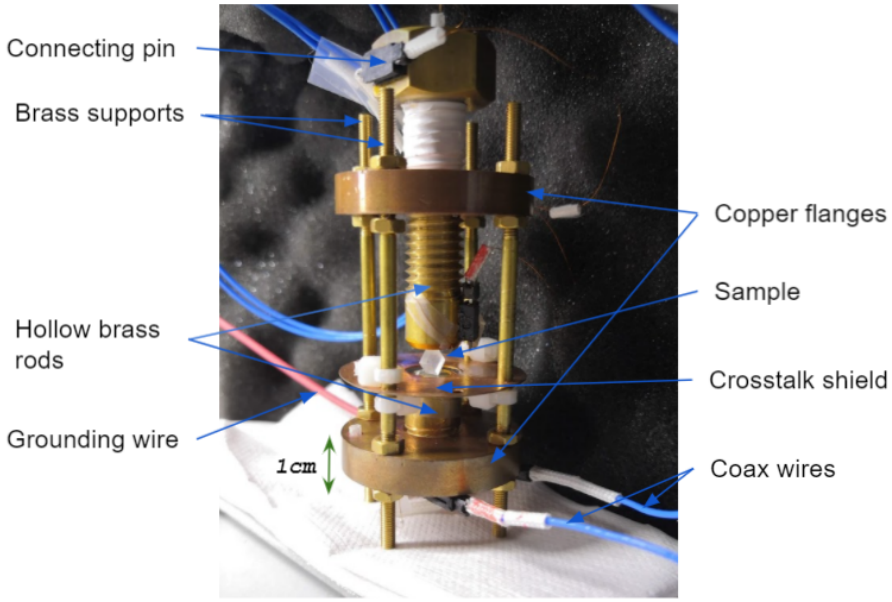

(a) The RUS sample holder with a sample and electric connections

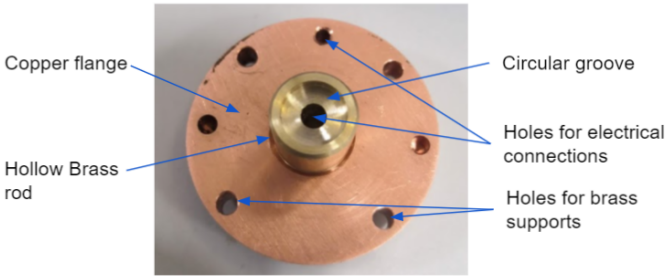

(b) An assembly of a copper flange and a hollow brass rod (before fitting transducer)

Figure 3.3: The low temperature RUS sample holder design

The construction details along with dimensions of each component are included in the appendix.

3.2.2 Transducers assembly

There are two transducers in the above sample holder, with each one of them fitted in a circular groove (Fig. 3.3(b)) made on one end of the brass rods. Before assembling them into the brass rods, these steps are followed: (a) electrical contacts on both sides of the transducers are made by using a silver paste and copper wires. When making the contacts on a transducer, one contact is made near the transducer's rim to allow for some space for mounting a sample. Also, cotton buds dipped in toluene are always used to clean in case of two conducting faces of a transducer are shorted by silver particles overflowing on the rim; and (b) to prevent electrical shorting between a transducer side and the conducting groove's face, GE-varnish is painted and dried, and a thin Teflon disc is placed in between the transducer and groove's surface on both brass rods. Then, the transducers are taken for assembling. Firstly, two wires that come from the back terminals of the transducers are taken out through the brass rods' hole. Next, all wire ends, which are to be connected to the ac voltage source and LIA through coax cables, are soldered to some connecting pins. Lastly, vacuum grease is used to fix the transducers in proper places. One advantage of going with vacuum grease instead of hard mounting here is that the grease acts like cushions to the transducers; hence, a weak contact between the sample and transducers is achieved easily.

When the transducers assembly is completed, all sample holder components are put together to obtain the whole sample holder setup, as shown in the previous subsection. To reduce the coherent pickups of EM noise, a crosstalk shield made of copper is put in between two opposing faces of the transducers while setting up the holder. Through the central hole of this shield, the RUS sample is kept in contact with the transducers for the measurements.

3.2.3 $LiNbO_3$ Transducers

To be able to excite stress to the sample, either a piezoelectric or ferroelectric material that can give compressional modes is required. A Z-cut or 36 degrees rotated Y-cut $LiNbO_3$ single crystal meets this above requirement [27][28]. Two Au/Cr coated, Z-cut $LiNbO_3$ piezoelectric crystals have been chosen as transducers in our sample holder. To measure the natural frequencies of the sample, these transducers should be operated at off-resonance frequencies; otherwise, their resonance will intrude [5]. Consequently, before starting our experiments, our $LiNbO_3$ crystals have to be characterized.

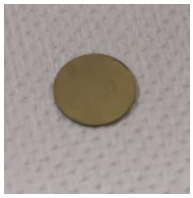

Figure 3.4: Lithium Niobate ($LiNbO_3$) disc with Au/Cr coat

Firstly, we confirm that the transducer crystals are Z-cut through XRD analysis. Next, using a Fabry-Pe′rot based AFM (Atomic Force Microscopy) instrument in the Nano-Mechanics lab Nanomechanics lab at IISER Pune headed by Dr. Shivprasad Patil, an experiment is performed to check if there is a compressional mode or not on the crystals [29]. In this experiment, interference patterns due to the partially reflected incident rays in optical fiber and purely reflected rays from one face of a piezo, driven with a sine ac voltage at different frequencies, are observed through the fiber interferometer. If there is any vibration along the poling axis of the piezo crystal, a change in the pattern, which is again converted into an oscillating current or voltage response, will be seen, thus confirming the presence of a compressional mode. The experimental results in Fig. 3.6 clearly show that there is a compressional mode. Besides, the theoretically and experimentally calculated amplitudes (~ 0.3 to 0.5 $\mathring{A}$) of the vibrations are found to be very close, which again supports the claim.

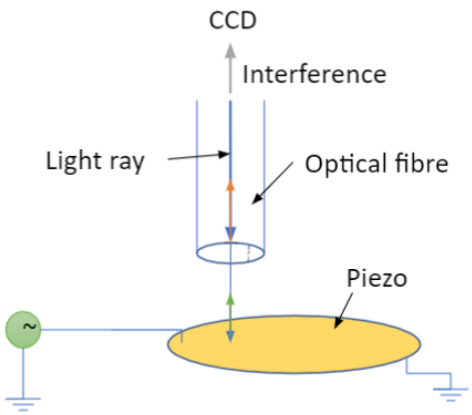

Figure 3.5: The schematic of Fabry-Pe′rot based AFM. The green arrow, the light ray reflected from the piezo surface, and the orange arrow, the light ray reflected from the optical fiber's tip, interfere in the optical fibre. The presence of a compressional mode of the piezo at a particular frequency changes the path length between the piezo and optical fibre tip, producing a change in interference pattern.

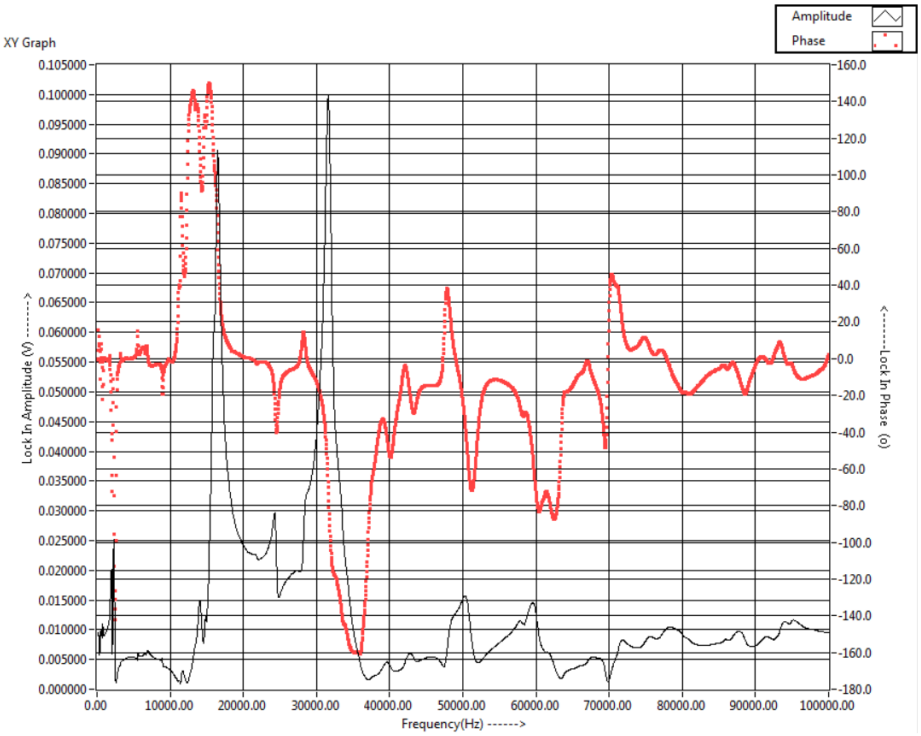

Figure 3.6: Amplitudes and phases of the piezo vibrations measured till 1Khz through the interferometer. The change in amplitudes show the presence of a compressional mode.

As a continuation of characterizations, another crucial experiment is also conducted to determine the resonance frequencies of the crystals. Any piezo or crystal oscillator is usually represented by an equivalent circuit known as the Butterworth Van-Dyke model, which consists of an LCR circuit and a shunt capacitor. So, a piezoelectric crystal has two resonance frequencies- (a) series resonance frequency, when the LCR part resonates due to reactances of the inductor and capacitor are the same but opposite and (b) parallel or anti-resonance frequency, when the whole circuit becomes like RC tank circuit and resonates. During series resonance, the effective admittance is maximum, and during parallel resonance, the effective admittance is minimum [30][31]. Using the simple circuit in figure.6, which involves a function generator and LIA (automated with the LabView program from section. 3.1.2), the admittances of the crystals can be measured indirectly across a range of MHz frequencies and the resonance frequencies can be determined. Thus, from this experiment (Fig. 3.9), we find the resonance frequencies of the two $LiNbO_3$ crystals are nearly 17MHz (same). In our RUS scans, the piezoelectric transducers will be typically operated below this frequency i.e., 17MHz. It is important to take note that phase changes when resonances occur.

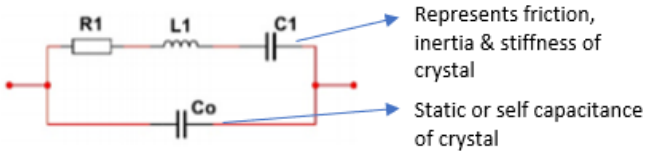

Figure 3.7: Butterworth Van-Dyke (BVD) model of a piezoelectric crystal

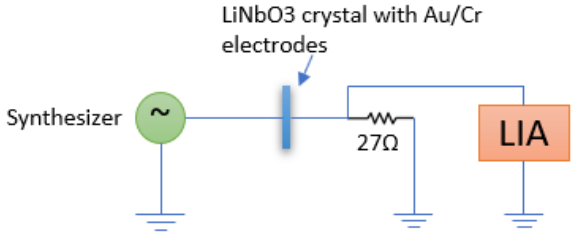

Figure 3.8: Circuit diagram for the resonance frequency determination. AC sine voltage of 1Vpp is passed through the crystal at different frequencies, and the corresponding voltage dropped across the 27 ohms resistor is measured.

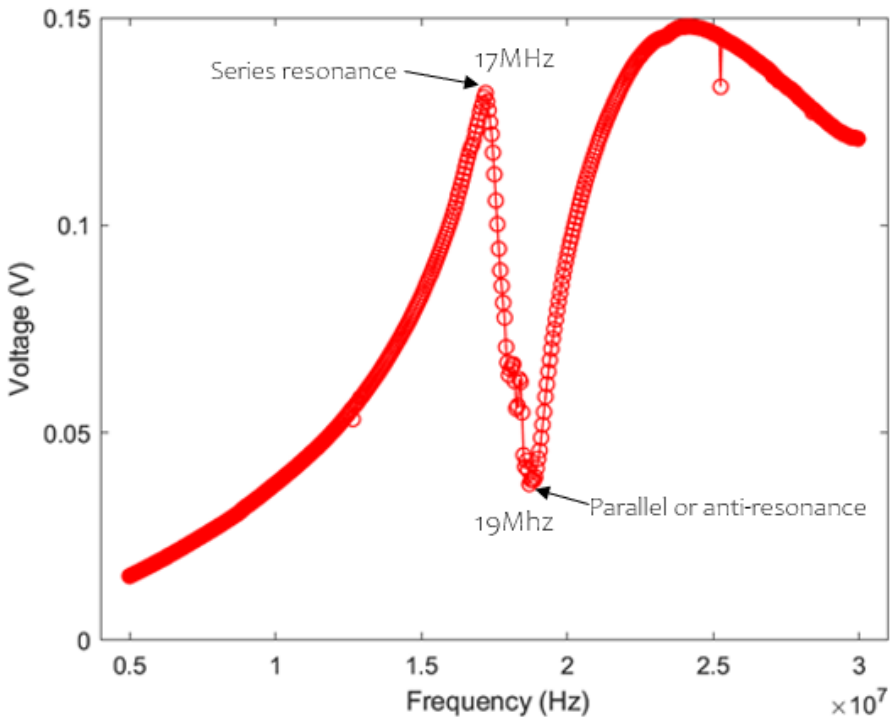

(a) Frequency vs Voltage measured across the resistor

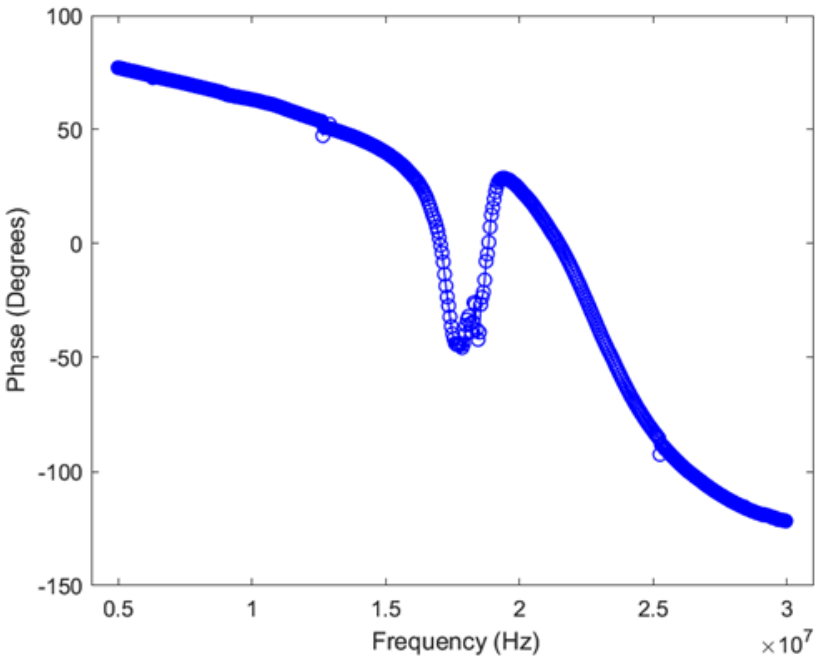

(b) Frequency vs Phase

Figure 3.9: The resonance and anti-resonance of our $LiNbO_3$ transducers. At 17MHz and 19MHz, the abrupt changes in both the measured voltage signal and the phase confirm that there are resonances at these points.

3.3 Sample preparation

In RUS, sample specimens with well-defined geometrical shapes should be prepared so that the analysis code can use the shape information to do the computations accurately. Among the wide variety of regular shapes such as spheres, cylinders, ellipsoids, etc., which are possible to make, a rectangular parallelepiped (RPR) is the easiest geometry that can be carved out of any material. So, samples prepared for RUS are mostly RPR shaped. For anisotropic materials like single crystals, it is suggested that the samples be cut with the crystallographic axes parallel to RPR edges (except for hexagonal symmetry crystals where only the sixfold symmetry axis should be along one edge) [5]. Deviation of edges directions from crystallographic axes gives rise to cosine errors in the computed results [3]. In isotropic or polycrystalline materials, we don't have to bother about crystallographic orientation. Sintered pellets made from well-grinded polycrystalline material can be treated as isotropic and taken for cutting and polishing.

Furthermore, it is required for the sample to be homogenous. Flaws inside like cracks or voids are considered as inhomogeneities that can cause high energy dissipation during a resonance. In addition, the sample surfaces should be polished and free of any contaminants.

3.3.1 Material selection

Potassium Dihydrogen Phosphate or KH_2PO_4, in short KDP, is an interesting hydrogen-bonded material with piezoelectric, dielectric, ferroelectric, and nonlinear optical properties. It exists in a paraelectric phase with tetragonal symmetry at room temperature [32]. But, below 123 K, it changes to a ferroelectric phase with orthorhombic symmetry [33]. This polymorphism allows us to observe and investigate the temperature-dependent structural transition by going at liquid nitrogen temperature in our RUS setup. And, KDP single crystals can be grown easily from their aqueous solutions by the slow evaporation method at room temperature [34][35]. So, it is an ideal material to start with for RUS test runs.

In subsequent sections, the protocols for growing, cutting, and polishing KDP single crystals will be discussed in detail.

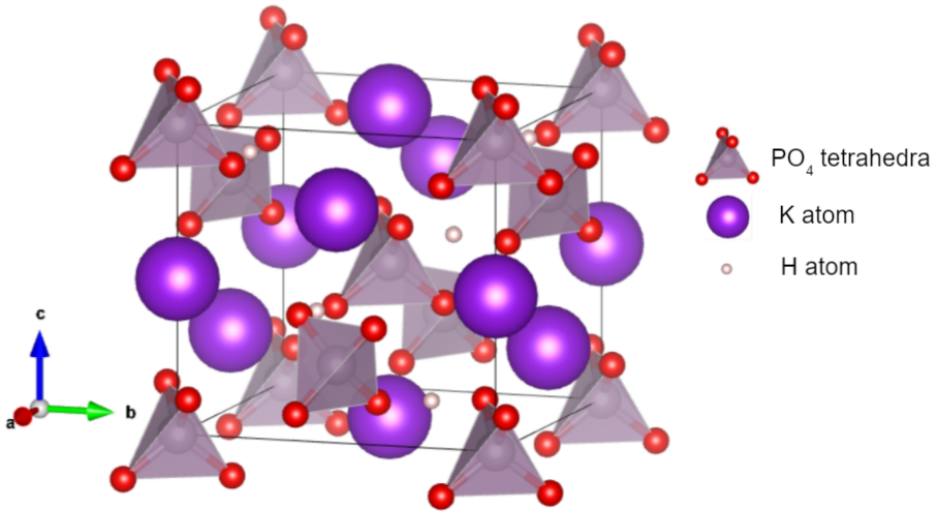

(a) The KDP unit cell structure

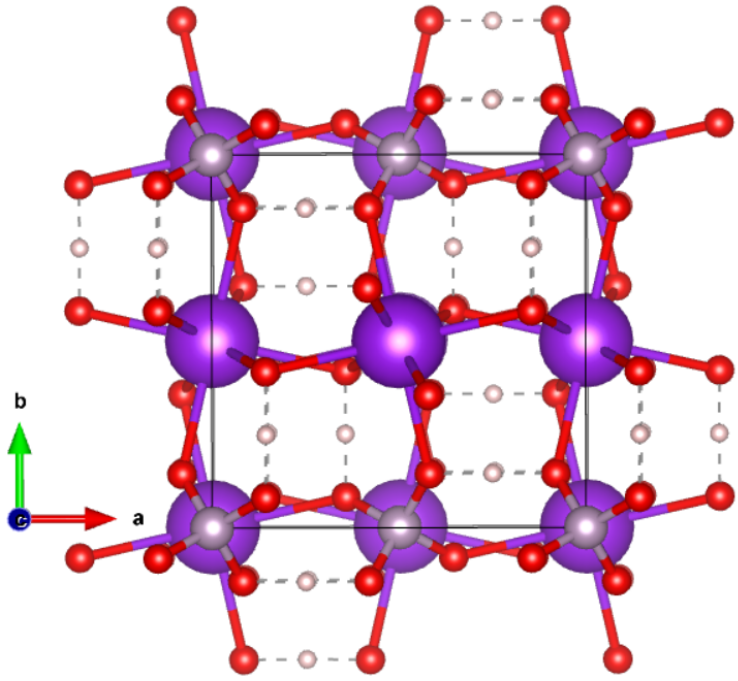

(b) The structure after including all bonds but along the c axis

Figure 3.10: The room-temperature structure of a KDP crystal, which belongs to the class $\bar{4}2m$ of tetragonal symmetry with space group $I\bar{4}2d$. The lattice parameters $a = b = 7.44\mathring{A}$, $c = 6.97\mathring{A}$, and Z (formula per unit cell) and density are 4 and $2.34g/cm^3$, respectively [1]

.

3.3.2 Crystal Growth

Slow evaporation of a supersaturated solution, a simple but quite effective technique for growing KDP single crystals, has been followed here. Along the way, we have also tried some tweaks to get the best out of the technique. Firstly, about 30g of commercially available raw KDP with high purity [SD Fine Chem Ltd.] and 200ml of Milli-Q water are added into a clean glass beaker and agitated using a magnetic stirrer till the solute dissolves completely. The solution is then heated up nearly to the boiling point of water on a hot plate. In no time, evaporation of water starts making it saturated slowly. A glass rod is dipped inside and scratched on the beaker wall for checking crystallite formation every 5-10 minutes. Once the solution becomes slightly viscous with crystallites forming over the glass rod, the beaker is removed from the hot plate. The solution is now supersaturated. This happens when the volume level drops to roughly 95ml in our case. Then, it is allowed to cool down for some time at room temperature before keeping inside a dark, soundproof, mechanical disturbance-

free closed cupboard. This cupboard has been specially designed with soundproof acoustic foams on the walls and a styrofoam block on the surface.

After 48 hours, the beaker is taken out from the cupboard to look for crystals. If only a few crystals are lying well-scattered on the bottom of the beaker, then the beaker is kept inside the cupboard again to continue the growth. Often, crystal clusters are also found in the solution. If the clusters are big and appear in all corners, it is always better to start afresh from the beginning because it is far less likely to get good single crystals from such clusters. But, this does not mean that we have to prepare a new solution. We can still use the old one. To use it, firstly, the grown crystals are dissolved by adding a little water and stirring. Later, it is brought to the supersaturated stage and kept for cooling and crystallization inside the cupboard. This process is repeated until isolated crystals with very few clusters are formed on the bottom. Once formed, the beaker is put inside the cupboard to resume the growth. Depending on the desired sizes, the crystals can be removed after some days or kept further for growing in the solution. KDP single crystals are thus harvested from this growth solution.

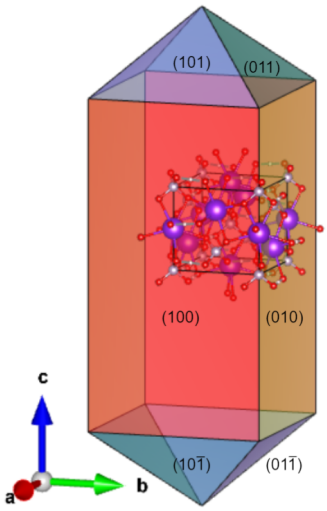

Figure 3.11: The ideal KDP crystal shape with prismatic faces and bipyramidal ends

The ideal shape of a KDP crystal is prismatic and bipyramidal, as shown in Fig. 3.11. However, in our work, two specific growth habits are found quite common. In Fig. 3.12, the related morphologies are illustrated with two fully grown crystals. Crystal A is prismatic and pyramidal, while crystal B is prismatic and half pyramidal. It can be mentioned that these morphologies greatly depend on the rate of cooling, concentration gradient, pressure, etc. In

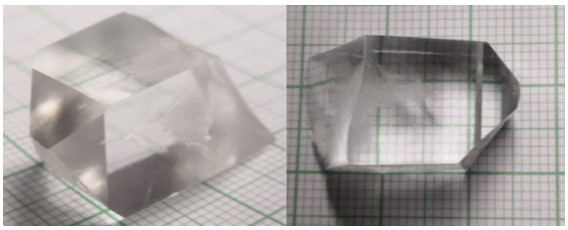

(a) Crystal A with dimensions $\sim 2 \times 1.2 \times 1.4 cm^3$

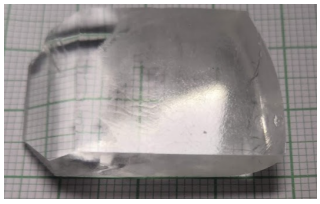

(b) Crystal B with dimensions $\sim 3 \times 2 \times 0.5 cm^3$

Figure 3.12: Grown KDP single crystals with their dimensions

both crystals, cloudiness resulting from tiny cracks can also be seen in one end. Mechanical vibrations and impurities could account for such cracks. However, the transparent portions of the crystals which are devoid of cracks can be used for our sample preparation.

There are few problems during the whole procedure except one -widespread clustering that can make all efforts futile. To deal with this problem, two major causes for clustering have been identified after several trials and close observations. The first cause is making the solution supersaturated overly by prolonged heating. When the saturation goes beyond a level, multiple nucleations occur right after removing the beaker from the hot plate. Also, some of them will give rise to crystallites that float on the relatively colder top surface of the solution. When these floating crystallites grow bigger and fall on top of one another, the clustering starts. Therefore, the beaker should be removed as soon as the supersaturation stage is reached. The right point of supersaturation can be determined with some hits and trials. The second one is the dust falling into the solution. Since nucleations will occur on the top region of the solution when dust falls into it, there are still chances of some crystallites falling on top of other crystallites that formed on the bottom, which may again lead to clustering. This one can be taken care of by filtrating the supersaturated solution with filter papers if any crystallites appear on the top surface.

It is also found that by hanging seed crystals in the solution using cotton threads or fishing lines, the clustering problem could be solved easily. However, as cotton fibers and

the chemical composition of fishing lines can become impurities in the crystals, we do not pursue this route.

3.3.3 Crystal Cutting and Polishing

Crystal B is picked for our sample specimen preparation. Being an anisotropic material, its crystallographic axes' directions must be defined before cutting out an RPR. A goniometer is required normally to orient if crystals are of irregular shapes, but it is not needed for our KDP crystals with well-defined shapes. Comparing the shape of the grown crystal to the ideal shape, we expect the c axis to be along the pyramidal ends, and (100) and (010) to be on prismatic faces. Still, it is only confirmed by performing Laue diffraction on all crystal faces. Once the directions are known, the bulk crystal is fixed on a cutting steel block using amber, and its transparent portion is cut off along the (001) or ab plane by using a low-speed diamond saw (Buehler-Model). Lines are marked properly on that cut piece to keep track of the crystallographic axes, and then a smaller piece is taken out from it by cutting along the ca and ab planes (Fig. 3.13 (a)).

In the next step, the (010) prismatic face (can be done with (100) too) on the smaller piece is chosen as a reference and fixed to the cutting block in a way that the saw can cut along two different crystallographic planes viz. the ab and bc planes. Then, four faces that are perpendicular to the reference face are cut. As mentioned earlier, it is essential to make the crystallographic axes parallel to the edges. A light polish on $(0\bar{1}0)$ side after the cutting brings the smaller piece to a proper RPR with the edges lie along the crystallographic axes. Furthermore, some RPRs are also cut out of the portions left from the last cuttings by following the above procedure.

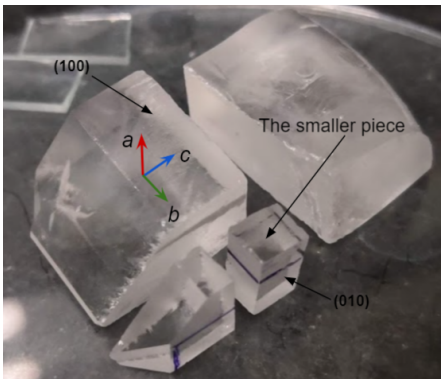

(a) The crystal B after cutting

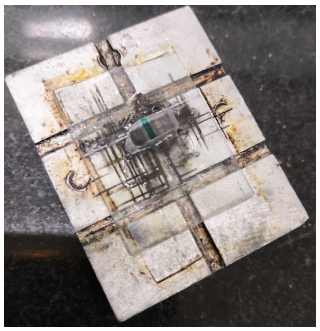

(b) A crystal piece with a green mark, fixed on the cutting steel block

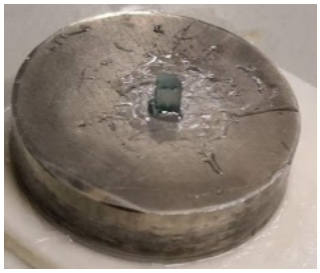

(c) A crystal piece, fixed on a steel disc of lapping fixture with amber

Figure 3.13: Some cutting and polishing stages of sample preparation.

KDP crystals are extremely fragile oxide materials. Even in a little harsh physical condition (like mechanical stress or heat), the crystals tend to get cracks. So, the temperature of the hot plate is always kept below 140 degrees celsius when melting the amber. During all cuttings, the rpm of the saw is kept low, and the blade is wetted with isopropyl alcohol (IPA) to reduce mechanical vibrations. And, the amber residues on cut crystal pieces are removed only by dissolving in acetone.

The cut RPRs usually have a very rough surface. For polishing, a precision lapping and polishing machine (MTI, Model UNIPOL-810) is used along with a special lapping fixture (South Bay Technology). And, it is reported elsewhere that a 600 grit paper will do a fine job for polishing the sample of 1 mm size [5]. A SiC circular 600 grit paper (from Buehler) is then used for polishing all faces of the KDP RPR crystals.

Firstly, an RPR is mounted on a steel disc of the lapping fixture using amber. The amber should be thinly spread when it is melted because any uneven thickness of this sticking material between the RPR face and the steel disc can lead to tilting of the polished face. Then, the lapping fixture is put on the polishing machine, and by setting a low rpm, one face is polished. Putting a few drops of IPA during polishing is found helpful in protecting

the sample edges and corners. Following the same procedure, all other faces of the RPR are also polished. Lastly, acetone is used to clean the amber residue and other contaminants.

After the polishing process, Laue diffraction patterns for all faces of the RPR are taken to check if the crystallographic axes are still along the edges and impurities or interior cracks are present. The patterns show most faces are still ok but for one or two faces with some slight tilts. The tilted faces are lightly hand-polished using a ceramic tweezer under a light microscope, and Laue patterns are retaken. Under the microscope, KDP crystals being transparent, internal cracks are also checked. Except for rough edges and slightly broken corners, no other flaws are observed. Once the desired shape, quality, and conditions on crystal directions are achieved, the sample is kept in a small flask filled with cotton balls. In this fashion, some RPR samples of increasing sizes are polished and characterized for our RUS study.

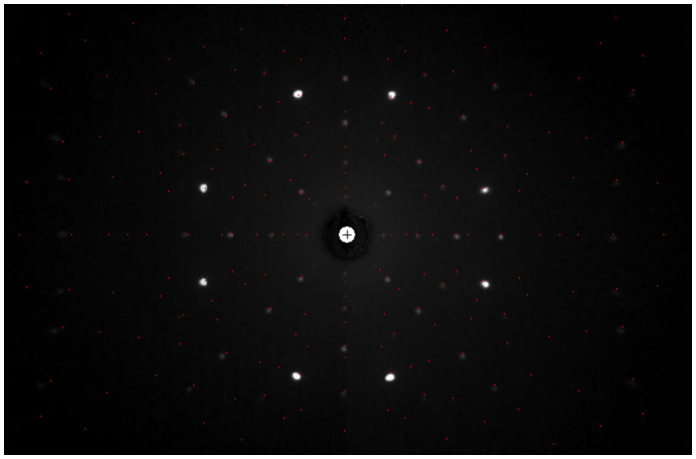

(a) along 001 direction or c-axis, showing a four-fold symmetry of reciprocal lattice points

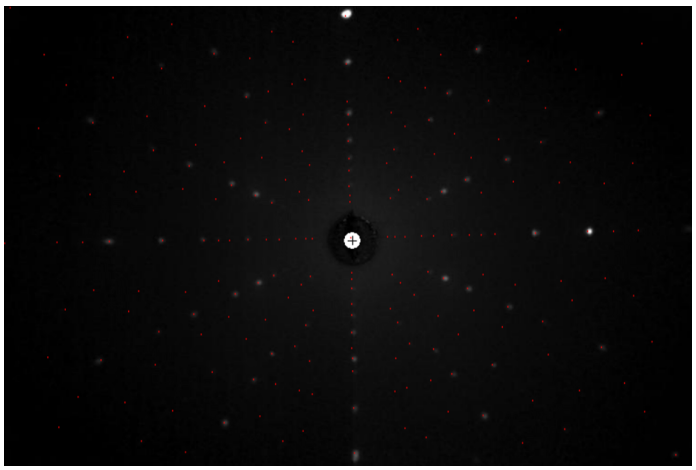

(b) along 010 direction or b-axis, showing a two-fold symmetry of reciprocal lattice points

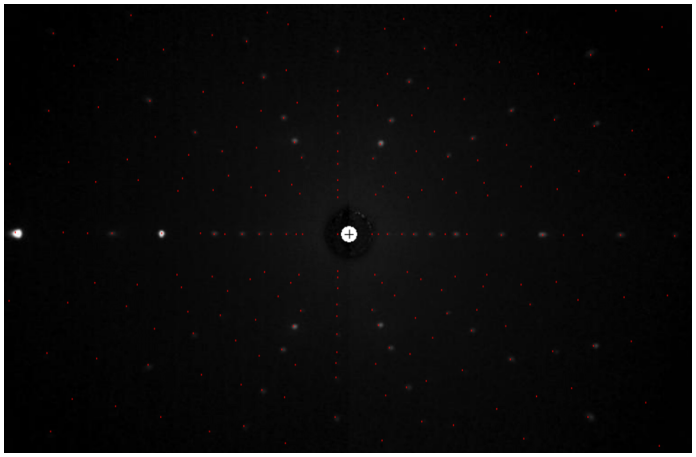

(c) along 100 direction or a-axis, showing a two-fold symmetry of reciprocal lattice points

Figure 3.14: The experimental Laue Diffraction patterns (white spots in the dark background) are taken using Back-reflection method along the three different crystallographic axes of a KDP (having tetragonal system) RPR sample. The simulated Laue patterns are the red spots, produced using OrientExpress software.

Perpendicularity and parallelism of the sample faces are thought to be big concerns in the RUS analysis [22]. So, some well-polished RPRs with face tilts more than 2 degrees are excluded from our RUS study sample set, leaving us only with two perfect RPR samples. The analysis of the tilt angles is done with the OrientExpress software, specially designed for crystallographic orientation analysis. Later, one more RPR sample is prepared from another parent crystal (not crystal B) with interest to compare the RUS scan results too. In the end, we have those three samples ready for mounting in the sample holder.

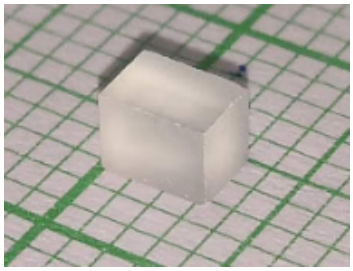

Figure 3.15: A polished RPR sample

The dimensions and densities of the above three samples will be required in elastic constant calculations. So, the dimensions are measured by using a Vernier Caliper, and the densities are determined from the mass by volume formula using measured mass. An impor-

tant point that might be noted is that the length, breadth, and thickness of all three crystals are made different to break any accidental degeneracies in resonance peaks [5].

Sample number	Dimensions (cm)	Mass (gm)	Density (gm/cm^3)
1	$0.252 \times 0.221 \times 0.187$	0.0238	2.28
2	$0.324 \times 0.253 \times 0.224$	0.0417	2.27
3	$0.339 \times 0.333 \times 0.249$	0.0638	2.27

Table 3.1: Some physical properties of the three samples

3.4 Measurement procedures

Before starting the RUS scans of KDP samples, it is important to determine the background noise level due to RF interferences among the wires and EM cross-talks between the transducers. So, rough scans are performed by keeping the sample holder inside a metal box (Faraday Cage) but without putting the sample. Mention can be made that the metal box, the sample holder, and the instruments are all grounded at a common point to prevent any ground loops.

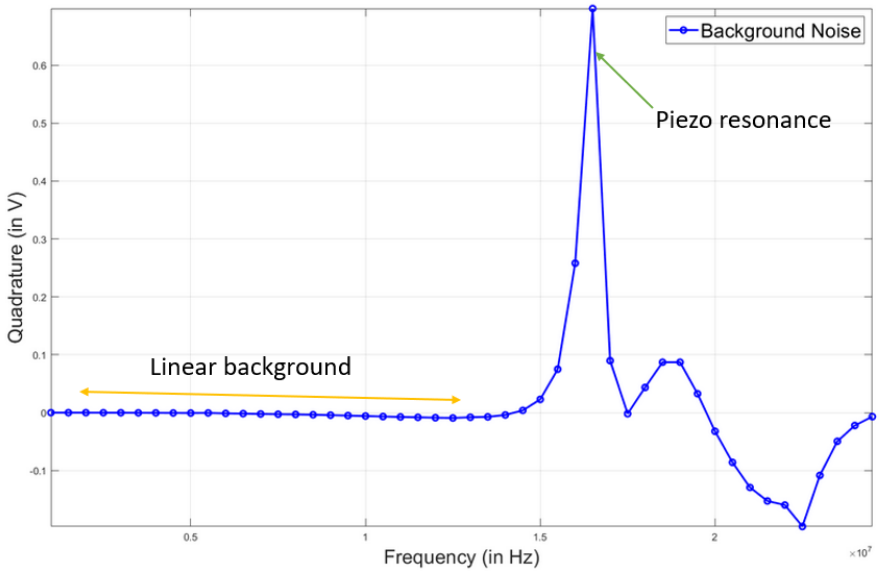

Figure 3.16: Background noise level before putting the sample in the sample holder. Notice the linear background below 15MHz.

The results show that background noise level decreases linearly without having any peaks (artifacts) until the resonance and antiresonance points of the transducers, as shown in the figure 3.16. Besides, the resonance peaks tell us that the piezos are working fine. But, sometimes, the resonance peaks do not appear in the scans. We find that when there is any kind of electrical shorting between the two faces of piezo, the current seeks the least path; hence the resonances diminish. So, it is highly recommended to clean the edges of the piezos with toluene or IPA without touching the contacts. If we get the resonance peaks, we are in shape to start our experiments.

Here, the procedures of performing a scan are similar to those of regular RUS - starting with mounting the sample in between two transducers, then driving a transducer with an ac signal, and observing the sample vibrations through the other transducer. After taking the scans, resonance frequencies are extracted by fitting the Lorentzian curves, and then inverse analysis code is used to determine the elastic constants from the extracted frequencies.

In the next two subsections, a brief overview of the sample mounting and the configurations used in the instruments is given.

3.4.1 Sample Mounting

There are three ways to mount an RPR sample -(a) with corners, (b) with edges, and (c) with faces. Among these three, the mounting with corners is the traditional way where the point contact can be made; hence the free vibration condition is met. Although, this mounting configuration has been pointed out as difficult and sometimes told to cause breakage of corners [5][22]. KDP crystals, being extremely fragile, this mounting will surely create problems. So, we move on with the remaining two ways of mounting.

Edge and face mountings are relatively easier. First, the gap between the transducers is set roughly close to the sample's dimension by adjusting the two brass rods as mentioned in subsection 3.2.1. Then, using a ceramic tweezer, we place the sample lightly in between two transducers, either with two faces or edges (preferably smaller ones). If any further change of the gap is needed, we can screw the brass rods in or out slowly, depending on the desired amount. Cares are always taken to make sure the sample just touches the piezos lightly and stays far from the silver contacts. Some pictures of these mounting configurations are shown in figure 3.18.

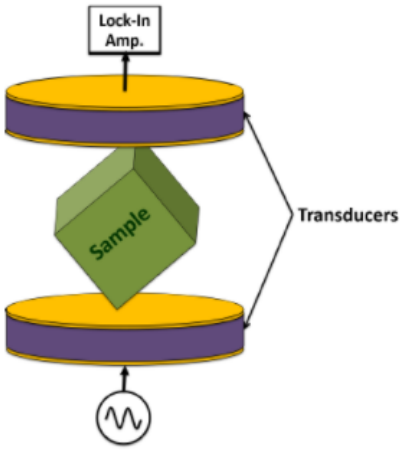

Figure 3.17: The traditional corner mounting configuration [22]

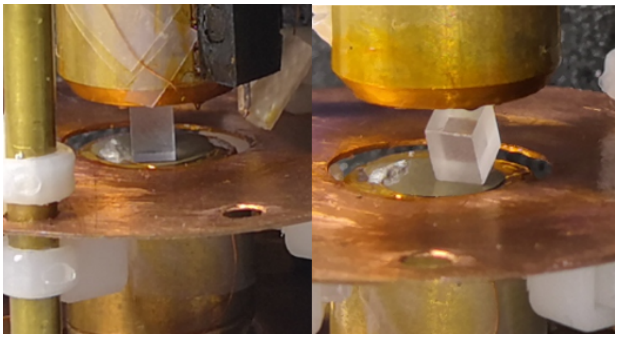

Figure 3.18: The sample mounting configurations: face-mounting (left) and edge-mounting (right)

We pay a high price when doing our experiments with the two preferable mounting styles. Because, some of the modes will have nodes on the faces or edges which will possibly be disturbed by transducer vibrations, meaning that some free vibration modes may be perturbed unintentionally. The whole point of corner mounting was to make contact with low symmetry points, which occurred to be the corners, where it is highly unlikely for a mode to have a node there. Fortunately, the brass rods and the vacuum grease make the transducers slightly non-parallel and create those required weak point contacts to our rescue. Thus, performing experiments on those mounting configurations is convenient.

During the RUS scans, it is found that some peaks (or modes) are missed, which might be due to many other reasons but primarily due to our mounting configurations. So, to reveal the missing peaks, the scans are done with multiple pairs of faces and edges on a sample.

3.4.2 Scanning for Resonance frequencies

After a sample is mounted, some configurations are set for operating the instruments on the LabView program, like starting frequency, frequency step size, transducer driving amplitude, time constant, reserves, sensitivity, etc. In all RUS scans, the transducer driving amplitude is kept at 10Vpp. The Lock-in amplifier is also configured at normal reserves and 100 ms time constant. However, the starting frequency, step size, and sensitivity depend on sample to sample. The frequency step size is usually determined by the width of the resonance peaks (and should be kept below the width). In our case, a step size of 50Hz or 100Hz is found to be enough to obtain all peaks in proper shapes.

Since we have a wide range of frequencies to search for the resonance peaks, we need to run the forward code, the one we mentioned in section. 2.4.2, for determining the starting frequency. The forward code requires the sample dimensions, density, and elastic constants from the literature. There are six elastic constants for KDP because it has tetragonal symmetry. So, after putting these values, we find the first mode or peak frequency. The computed frequency values are always in the hundreds of kHz range. Then, we set our starting frequency a little lower than the first peak frequency, and the RUS scan is done. In the scan, the amplitude (R), phase (θ), In-phase component (X), and Quadrature component(Y) are all measured.

Scans are done for all three samples on the faces and the edges to extract all possible modes. It takes around two weeks to complete the scans.

Chapter 4

Results and Discussions

4.1 Resonance peaks

The RUS resonance peaks are expected to look like Lorentzians with phase shifts [3][14]. After comparing some of our experimental peak shapes with the Lorentzians illustrated in figure 4.1(a), we can infer that the peaks observed in our scans are resonance peaks. Moreover, we find changes in a phase (θ) wherever there is a peak in the scans, which is a strong signature of a resonance. Each peak here corresponds to a normal mode of a sample.

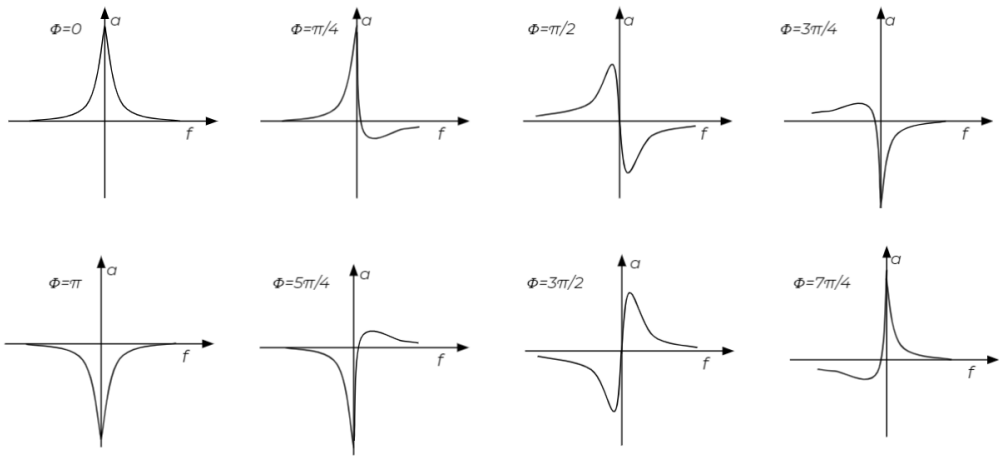

(a) Some Lorentzians with phase shifts (Φ); a is the amplitude and f is the frequency. It should be noted that the central frequency is not always at the peak extremum.

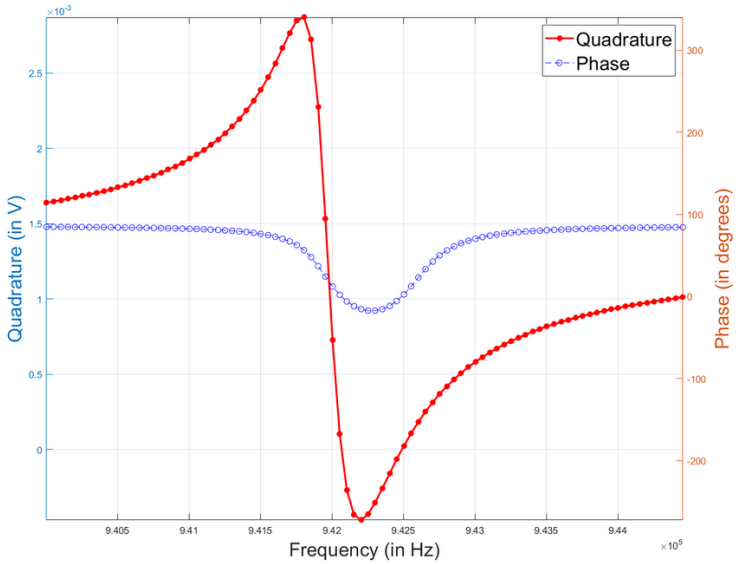

(b) An experimentally observed peak alsong with the phase curve

Figure 4.1: The experimentally observed peak in (b) is similar to the Lorentzian with a phase (Φ) shift of 90 degrees in (a). Also, the blue phase (θ) curve in (b) changes at the place where the observed peak appears.

It is to be noted that a linear background is always present in all the scans. This linear background pertains to the electromagnetic (EM) crosstalk between the two transducers. From the figure. 3.16, the linear background in the lower frequencies is also obvious. It is removed by using a function called 'detrend()' in Matlab so that we can plot and visualize the peaks better. Also, we use quadrature components (Y) of the scans for most of our analysis because this output is expected to have fewer crosstalk features.

4.2 Peak positions, intensities, and sample sizes

The reason for making our samples with increasing sizes (Table. 3.1) is to check if the peak positions and intensities are changed in the RUS scans when we change our sample. In theory, the resonance frequencies or spectra of a material are not unique. Because, even if the elastic constants are the same for samples made of the same material in different sizes, the differences in dimensions are going to give different resonance frequencies. To be clear, let us take two iron rulers, one shorter and another longer, and strike at one of the ends on both rulers; what will we see? The shorter ruler will vibrate at a higher frequency, while the

longer ruler will vibrate at a lower frequency. So, this means that the sample dimensions will determine the positions of peaks even if the samples are of the same material.

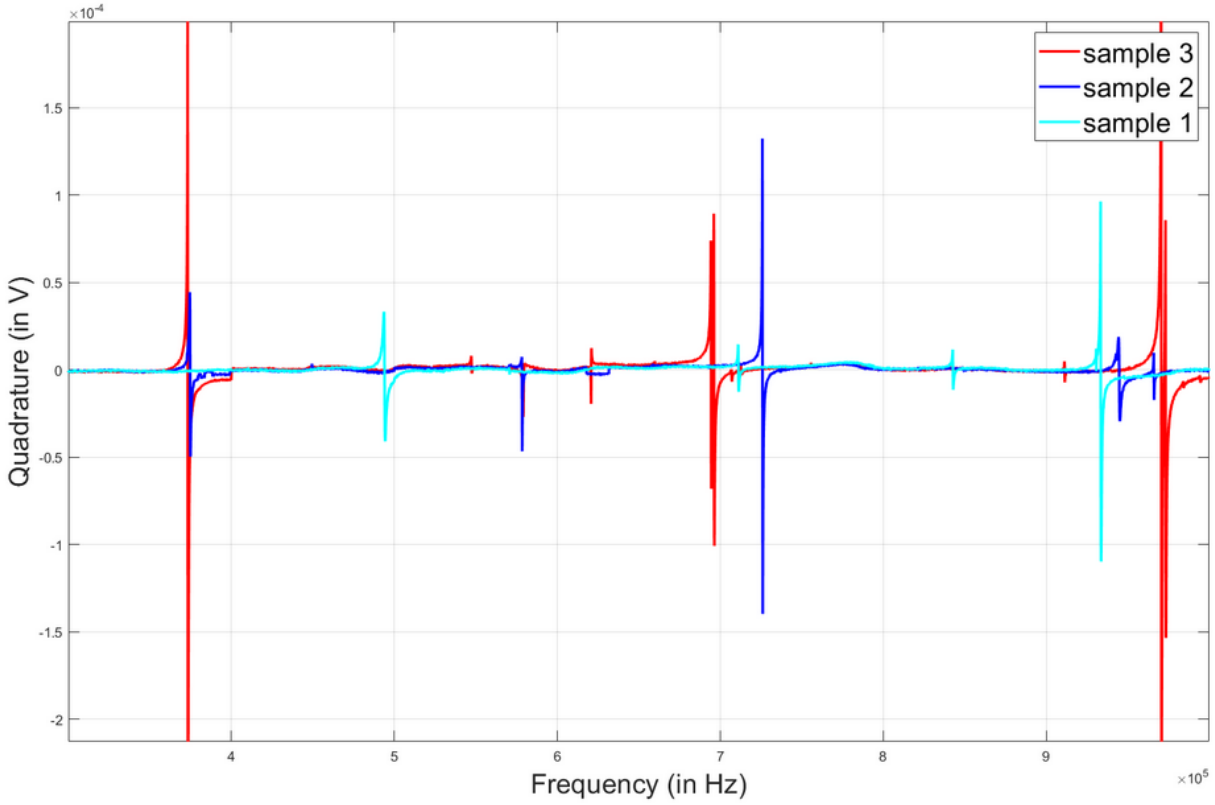

Figure 4.2: Frequency vs Quadrature signal plots for the scans of the three samples mounted with edges. The resonance spectra for the samples are different which is due to differences in sizes. Also, the peak intensities for sample 3 are more prominent than the other two samples.

As expected, we find our peaks positions are different for different samples confirming that the peaks in the scans are not due to artifacts as well as the resonance spectra of a material are not unique. To illustrate the above statement, we have shown a comparison of scans performed on sample edges in Fig 4.2. We notice that overall peak intensities in the figure become more prominent as the sample size increases. A possible explanation for this is the increase in contact areas between the transducers and the samples. The stress experienced by a sample is proportional to the contact area between the sample and the driving transducer. Also, the strain made on the receiving transducer is proportional to the contact area between the sample and the transducer. So, for a sample with longer edges, both the stress and strain are more significant, giving more prominent peaks.

Further, the smaller the sample size, the higher the resonance frequencies will be (i.e.,

The resonance spectra will be shifted to the higher frequencies range). In Fig. 4.2, the peaks of sample 1 (which is smaller than sample 3) are starting to appear at higher frequencies. A comparison of the leftmost part of the resonance spectra in Fig.4.2 is shown with their corresponding mode numbers to understand the shifting of the peaks in the table. 4.1 and Fig.4.3.

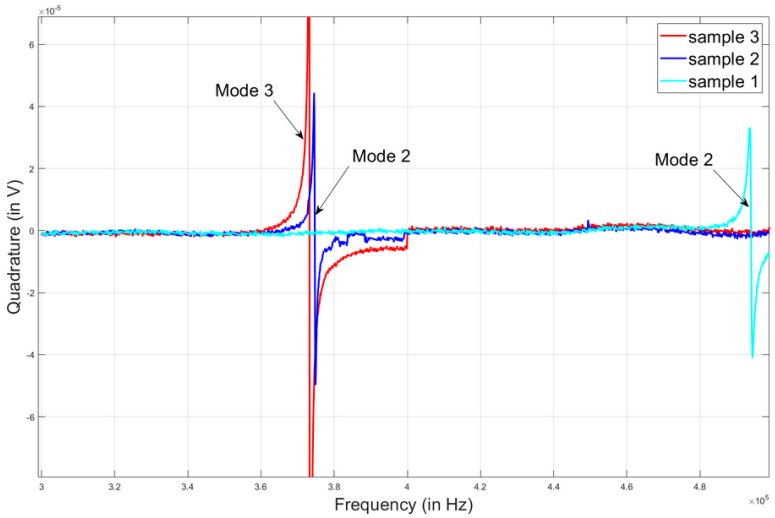

Figure 4.3: The leftmost portion of Fig. 4.1 (magnified) showing the peaks with corresponding mode numbers. The first red peak corresponds to the third normal mode of sample 3. This peak comes earlier than the peaks corresponding to the second normal modes (blue and cyan peaks) of samples 1 and 2.

Sample	Mode	Frequency(Hz)
1	2	494203
2	2	374701
3	3	373301

Table 4.1: The peaks to left as the sample size increases.

4.3 Reproducibility of the Peaks

In high-frequency measurements, getting spurious peaks or humps due to noise (maybe mechanical or EM) from the environment is not unusual. Therefore, we need to check the reproducibility of our data before going ahead. So, repeated scans are done on two samples viz—sample 2 and sample 3 after unmounting and remounting the samples. The two plots in the Fig.4.4 show the comparisons of the resonance spectra obtained from repeated scans.

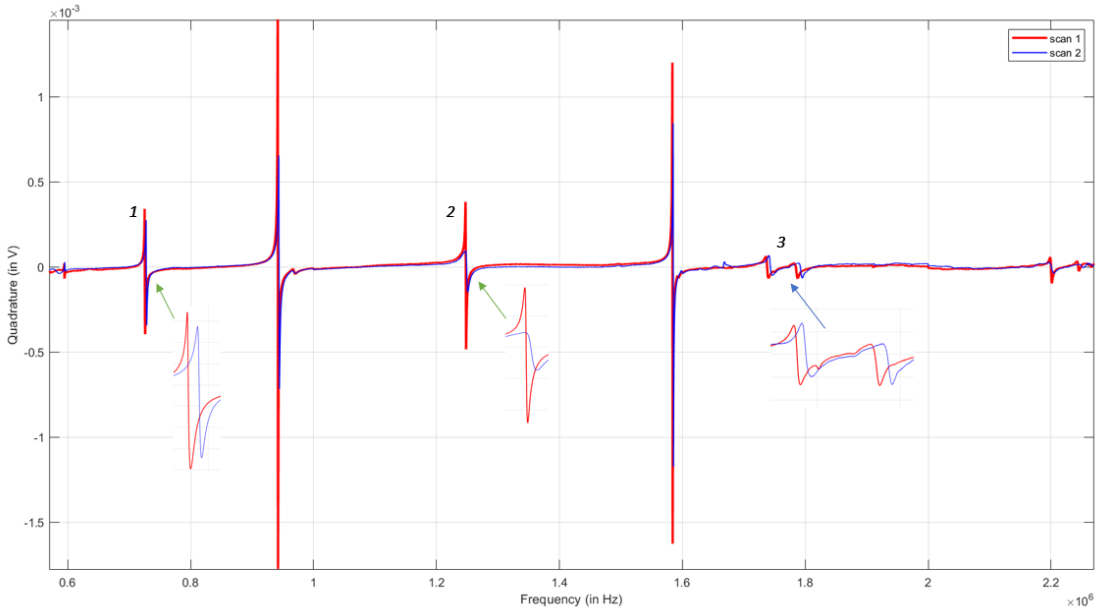

(a) Two scans on the same two opposite faces (c-axis) of sample 2.

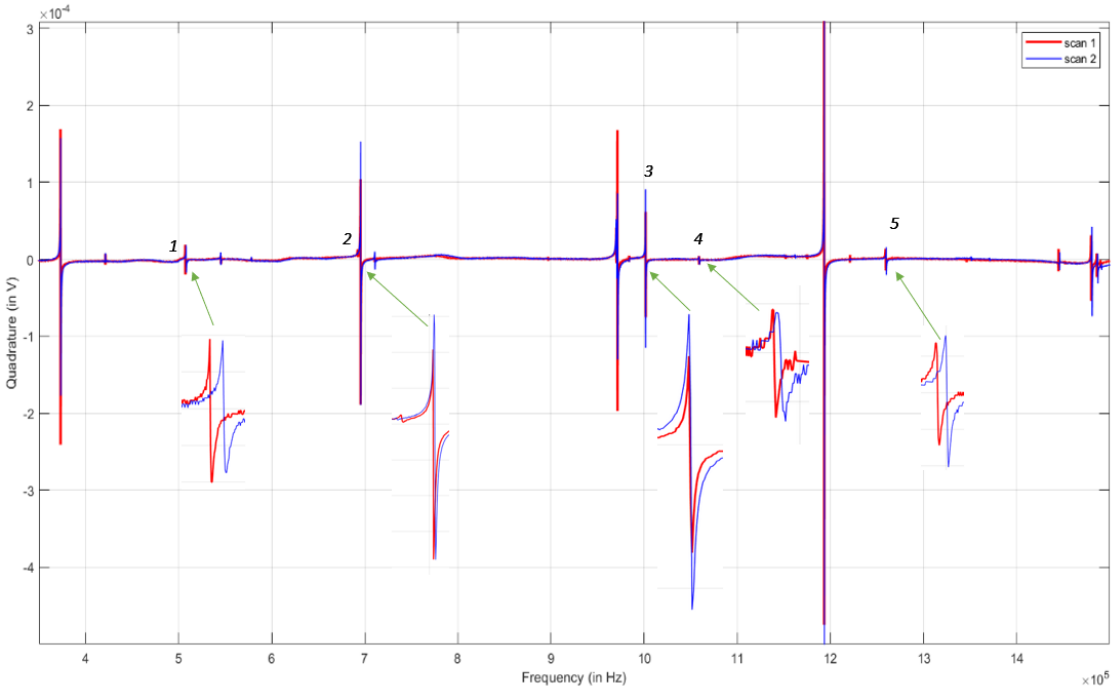

(b) Two scans on the same two opposite edges of sample 3.

Figure 4.4: Shown are the plots between frequency and quadrature for the repeated scans. Some peaks are zoomed in to see the shifting and overlapping of peaks. The peak shifts are found to be nearly 1kHz big. And, the differences in peak intensities for same modes in the plots are due to independent mountings where the contact areas and contact forces between the sample are not the same.

In the plots, the peaks are coming at the places they should be. So, we can say that our data is reproducible. But, some peaks are not occurring at the exact same frequencies. The shifting of the peaks in the left or the right is due to the mounting configuration. Whether it be edge mounting or face mounting, repeated mountings will have different contact points with the transducers. Some contact points may be on the nodes or antinodes of the sample vibration modes. So, the nodes or antinodes may be easily perturbed due to the transducer vibrations, and hence, the resonance frequencies may come up at different points. However, we found the shifts of frequencies are minor in two samples except sample 1. In samples 2 and 3, the peaks of a particular mode in different scans lie close to each other.

4.4 Resonance frequency and Q-factor extractions

Since the resonance peaks are reproducible, our next step is to find the peak positions. To find the peak positions, the peaks have to be fitted with a Lorentzian function. A typical Lorentzian function is given as:

$$a(f) = a_0 \left(\frac{\frac{f}{f_0}\cos(\Phi) + \left(1 - \left(\frac{f}{f_0}\right)^2\right) Q \sin(\Phi)}{\left(\frac{f}{f_0}\right)^2 + \left(1 - \frac{1}{f_0}^2\right)^2 Q^2} \right) \tag{4.1}$$

where A_o is the peak amplitude, Q is the quality factor, Φ is the phase and f_o is the resonance frequency is the amplitude . But, the experimental peaks are also usually associated with background noise (mostly fluctuating noise floors) due to electromagnetic interferences and mechanical vibrations. One background noise due to crosstalk has been already removed in the section. 4.1. To model the other remaining background noise, some higher-order polynomials are added, and the fitting function is modified as:

$$a(f) = a_0 \left(\frac{\frac{f}{f_0}\cos(\Phi) + \left(1 - \left(\frac{f}{f_0}\right)^2\right) Q \sin(\Phi)}{\left(\frac{f}{f_0}\right)^2 + \left(1 - \frac{f}{f_0}^2\right)^2 Q^2} \right) + \left(a_1 + a_2 f + a_3 f^2 + a_4 f^3\right) \tag{4.2}$$

Any curve fitting software can be used to fit a single peak or with more adjacent peaks

at a time. We have tried in Matlab, but unfortunately, the fittings are not good. So, we extract the frequencies through plotting and painstaking comparing every single peak with the Lorentzian shapes in Fig 4.1. The point on the x-axis where the amplitude axis meets the peak curve is taken as the resonance frequency. Two plots are shown along with the axes to give an overview of the process (Fig. 4.5). Although the process is tedious, the effort will be the same on the Matlab curve fitting tool too. Because, every peak has to be fitted by importing a particular range of the frequency and quadrature repeatedly. Until and unless a GUI (Graphical User Interface) for fitting Lorentzian curves is developed, the extraction of frequencies will remain strenuous.

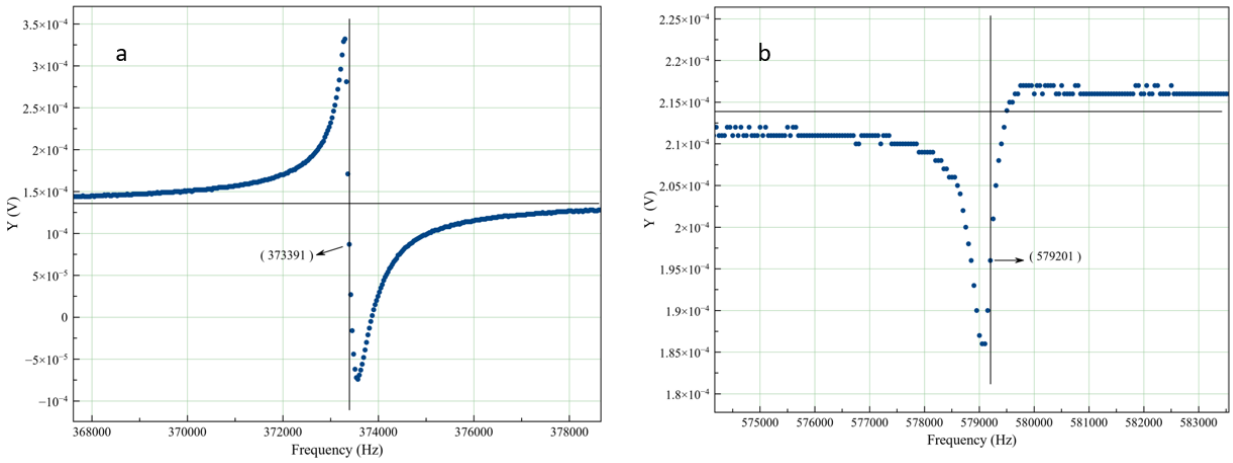

Figure 4.5: These are two examples of the extraction process of resonance frequencies. The point where the central line, parallel to the quadrature axis, meets the resonance curve is taken as the resonance frequency for that resonance peak.

The quality factor or Q factor is defined as the rate of energy loss in a resonator vibrating at frequency f, mathematically expressed as ($Q = f_o/\Delta f$) where Δf is the full width at half maximum (FWHM) of the resonance peak. The Q factors for some peaks have also been roughly calculated to give a fair idea of the peak size and attenuation of the resonance peaks.

Edge 1			Edge 1		Edge 2		Edge 2	
f	C	Q	f	C	f	C	f	C
373301	1	-	373391	1	373251	1	373501	1
423402	0	-	545533	1	421351	1	421402	1
524302	0	-	619512	1	507252	1	491102	0
547352	1	600	658512	1	545402	1	508102	1
579201	1	1200	692174	1	578253	1	545252	1
620752	1	-	695683	1	619452	1	578403	1
641503	0	-	710833	1	658152	0	619102	0
660002	1	-	754513	0	692404	1	691953	1
694353	1	1100	897492	0	695403	1	695552	1
696153	1	1100	909884	1	710602	1	710852	1
707003	1	1500	938594	0	754053	0	754153	0
712752	1	900	943214	0	896754	1	897104	0
755503	1	-	949874	0	909604	0	910352	0
848604	0	-	970124	1	970202	1	938002	0
874952	0	-	970964	1	971204	1	970004	1
911204	1	2000	992982	1	983804	1	970454	1
939704	0	-					971552	1
951004	0	-					984154	1
970552	1	1100					993454	0
973202	1	1200						
984154	1	-						
994404	1	-						

Table 4.2: Resonance frequencies f along with some Q factors of sample 3. C is the confidence value that tells whether a peak is clearly identifiable or not. Scans were done on two different opposite edge pairs.

In table 4.2, the resonance frequencies and some Q factors for peaks from sample 3 scans are shown. Some peaks are tiny, so to confirm their presence, we check for any signature in Frequency vs. phase plots too. If there is any signature in phase but not big enough in the Frequency vs. Quadrature plot, we have put a confidence value of 0. The confidence values are used as the weights of $G(x)$ in the non-linear fitting (section 2.4.2) performed through the Inverse code.

4.5 Forward code and Missing modes

Even though multiple scans with different mounting configurations are run to obtain all the modes, some modes are still missed. Firstly, we notice the possibility of missing modes during the extraction of the resonance frequencies as there are lots of gaps among the peaks. Then, we run the Forward code to check how many peaks have been missed because running

the Inverse code will be impossible if there are lots of missing peaks.

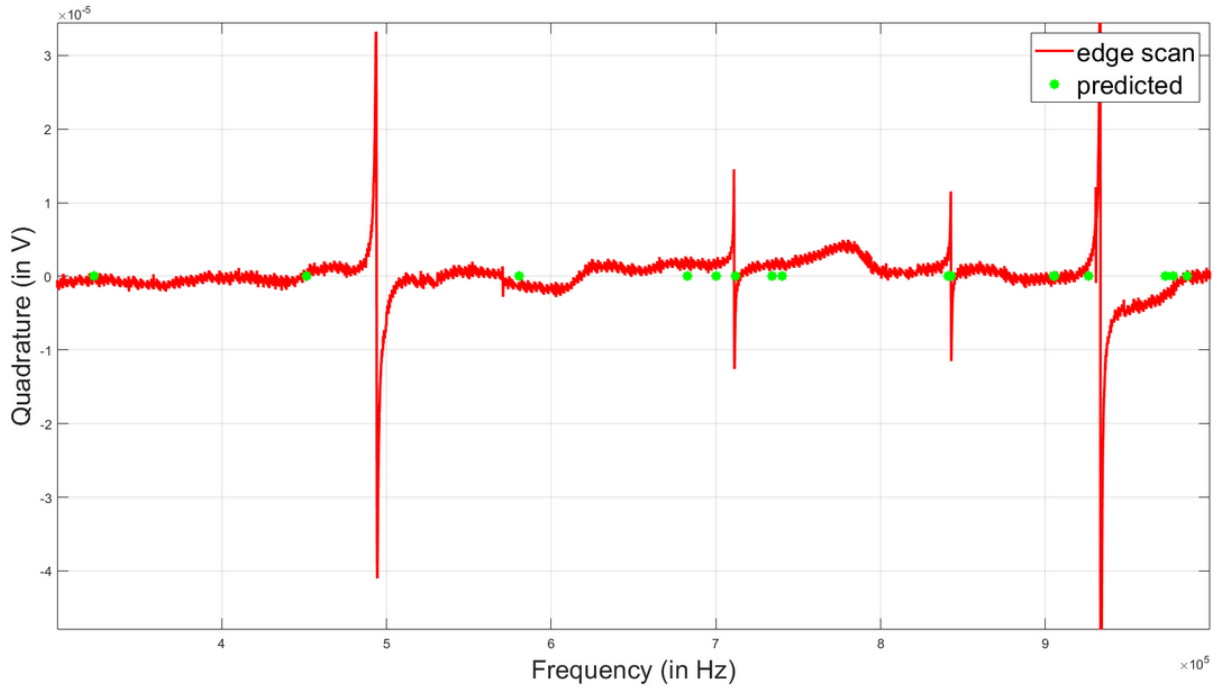

(a) Edge scan of sample 1. The green dots are predicted resonance peak positions.

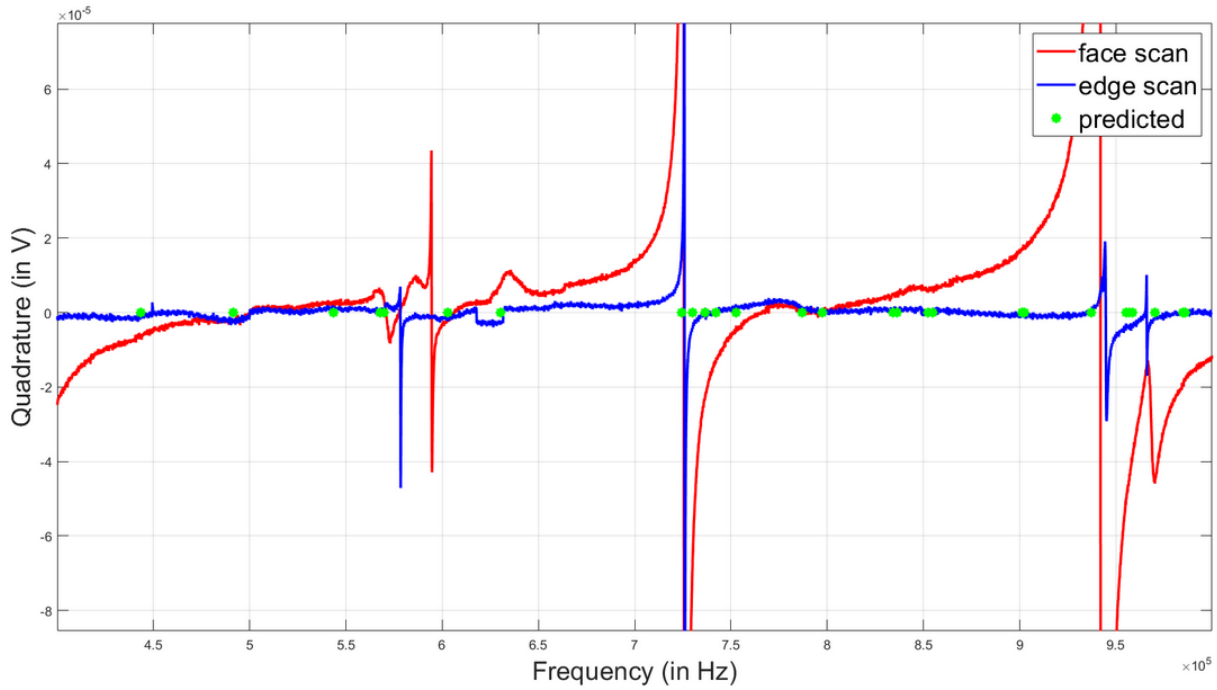

(b) Face and edge scans of sample 2. There are also tiny peaks that are not seen in the plot. The green dots are predicted resonance peak positions.

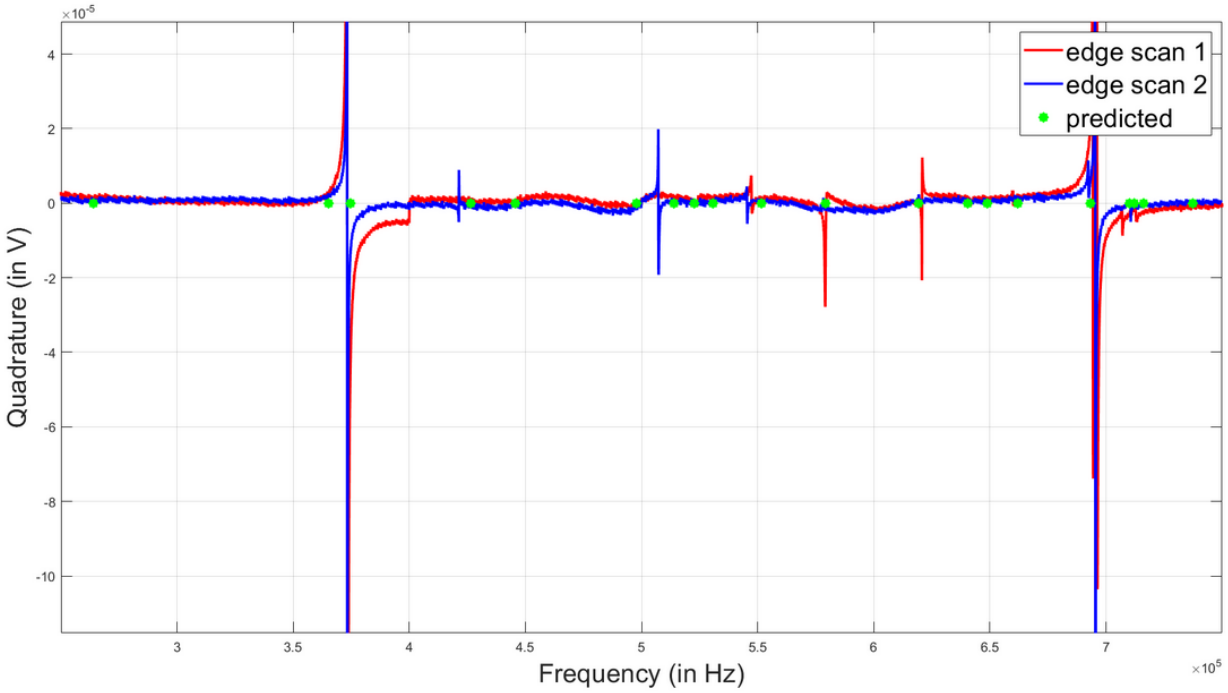

(c) Two edge scans of sample 3. Most of the peaks are prominent and lie close to their respective predicted positions (green dots).

Figure 4.6: Some peaks are not observed at the predicted positions. This is because of the preferable mounting configurations. Also, the predicted peak positions are shifted left or right to the observed peak positions. Two reasons for this: (a) the elastic constants, being intrinsic to the sample, can differ from sample to sample of the same material. So, we expect the resonance spectra to be slightly off from the predicted spectra. And (b) environmental factors like uncontrolled temperature and pressure can also give different spectra in repeated scans

The figure. 4.6 shows the predicted peak positions in green dots. For samples 1 and 2, the missing modes are more, partly due to smaller contact areas and the preferable mounting configurations. Moreover, it is also found that the number of missing modes is more in the cases of face mountings. The reason for this one is quite straightforward. As the face mounting will have more contact areas with the transducers, the free vibrations of the samples are disturbed more; hence more the number of missing peaks.

The Matlab programs for plotting the peaks with predicted frequencies and for comparisons are put in the appendix.

4.6 Elastic constants of KDP

It is said earlier that there are six elastic constants of KDP. The nominal values of those six elastic constants for the previous forward calculations were taken from a paper by Bantle et.al [36]. Here, for the inverse calculations, we will use the same nominal values again.

C_{ij}	C_{11}	C_{33}	C_{44}	C_{66}	C_{12}	C_{13}
Values (in GPa)	70.8	58.4	12.8	6.33	-3.83	15.5

Table 4.3: The nominal values of six elastic constants of KDP

Firstly, we make a .txt file consisting of the initial few resonance frequencies and their corresponding confidence values. After that, we put the arguments: the order of polynomials(N, the maximum power value of Visscher basis), dimensions, density, the shape of the sample, crystal symmetry, and elastic constants in a command line. Then, the inverse code is run iteratively till the chi-square value becomes very low. Once the value becomes low, we add two or three more frequencies in the above .txt file and rerun the code. Sometimes, if there is any missing mode, the chi-square value shoots up instantly. In such time, we have to guess the possible missing frequencies through hit and trial until the fitting is good enough. It is a lengthy semi-manual process. For the time being, we are in the stage of debugging some errors in the inverse code and simultaneously fitting our sample data.

4.7 Sources of errors

There are a few couples of sources that might affect our experimental results.

- Uncontrolled Temperature and Pressure: Our sample holder is kept inside a metal box with holes for electrical connections. So, any change in room temperature and pressure will also affect our measurements. The temperature change can lead to the sample's thermal expansion, changing the elastic constants and giving peaks at different frequencies. Also, due to air loading or pressure, the Q factor for most of the modes will be smaller. Although, according to Phils Spoor's thesis, the changes are reported to be small.
- Moisture content: Since KDP is hygroscopic in nature, our sample may adsorb some

water from the air moisture too. This water adsorption will break the homogeneity and alter the modes' displacements.

- Mounting configuration: Our mounting styles do not fulfill the free vibration condition. So, there will be some resonance frequency shifts and errors in computed elastic constants.

- Sample preparation: We put much effort into getting good samples. Nevertheless, breaking of the sample edges and unavoidable scratching on the sample's surfaces occur sometimes when polishing and mounting on the sample holder. Such breakage and scratches will indeed be reflected in our frequency measurements. We tried to handle the sample carefully to keep such occurrences at bay.

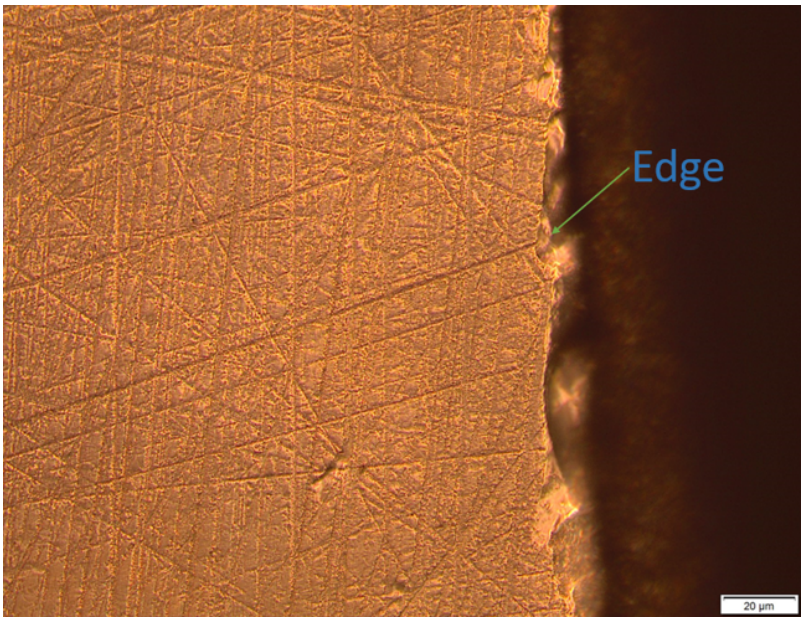

Figure 4.7: Showing the size of a breakage on an edge of a sample. The breakage occurs when mounting the sample with edges. The scratch lines on the surface are due to roughness of the grit paper, used in polishing the sample. Such a significant breakage makes the mode frequencies shifted.

Chapter 5

Conclusion and Future Work

We have presented a design of an Resonant Ultrasound Spectroscopy setup in this work. Along with some characterizations, the measurement of elastic constants through the technique has also been discussed. We have shown how to grow KDP single crystals and prepare samples for RUS. Though we have not computed elastic constants of KDP here, we have found that the predicted frequencies are very close to the experimentally observed resonance frequencies using the Forward calculation. We expect to fix the persisting problems in the Inverse code in a short time and compute elastic constants.

Along the way, we have come across many ways to improve the technique. In literature, most of the RUS scans are done with face mounting as the corner mounting is difficult. Here, we have tried and shown that edge mounting is a better option than face mounting as it reduces the chances of missing modes. We also believe that using a transducer, which has shear modes, can help in increasing the number of modes observed in the case of face mounting. Moreover, the use of vacuum grease is found to achieve weak contact between the sample and transducers better than any rigid mounting in transducer assembly. It also solves the accidental breaking of transducers, a major problem faced during sample mounting. The noise coming in our data has not been a big issue till now. Nevertheless, we will try to improve the electrical connections and perform the experiment in a vacuum to reduce the number of missing modes and increase the quality factors of peaks.

It is also our future goal to develop a GUI for fitting Lorentzian functions effectively. Having such a GUI will simplify the fitting of resonance peaks and save more time. And, we are trying if the technique can be extended for polycrystalline samples in our setup too.

Last but not least, the setup will be modified for low temperature measurements once we have completed the remaining part of the analysis with the KDP samples.

Bibliography

[1] RJ Nelmes, GM Meyer, and JE Tibballs. The crystal structure of tetragonal kh2po4 and kd2po4 as a function of temperature. *Journal of Physics C: Solid State Physics*, 15(1):59, 1982.

[2] Guangyan Li. *High temperature resonant ultrasound spectroscopy studies of thermoelectrics and other novel materials*, volume 72. 2010.

[3] Fedor F Balakirev, Susan M Ennaceur, Robert J Migliori, Boris Maiorov, and Albert Migliori. Resonant ultrasound spectroscopy: The essential toolbox. *Review of Scientific Instruments*, 90(12):121401, 2019.

[4] G Li and JR Gladden. High temperature resonant ultrasound spectroscopy: a review. *International Journal of Spectroscopy*, 2010, 2010.

[5] Albert Migliori and JD Maynard. Implementation of a modern resonant ultrasound spectroscopy system for the measurement of the elastic moduli of small solid specimens. *Review of scientific instruments*, 76(12):121301, 2005.

[6] A_ Migliori, JL Sarrao, William M Visscher, TM Bell, Ming Lei, Z Fisk, and R Gi Leisure. Resonant ultrasound spectroscopic techniques for measurement of the elastic moduli of solids. *Physica B: Condensed Matter*, 183(1-2):1–24, 1993.

[7] DB Fraser and RC LeCraw. Novel method of measuring elastic and anelastic properties of solids. *Review of Scientific Instruments*, 35(9):1113–1115, 1964.

[8] Harold H Demarest Jr. Cube-resonance method to determine the elastic constants of solids. *The Journal of the Acoustical Society of America*, 49(3B):768–775, 1971.

[9] Julian Maynard. Resonant ultrasound spectroscopy. *Physics Today*, 49(1):26–31, 1996.

[10] RB Schwarz and JF Vuorinen. Resonant ultrasound spectroscopy: applications, current status and limitations. *Journal of Alloys and Compounds*, 310(1-2):243–250, 2000.

[11] Robert G Leisure and FA Willis. Resonant ultrasound spectroscopy. *Journal of Physics: Condensed Matter*, 9(28):6001, 1997.

[12] Oleg Heczko, Hanuš Seiner, Petr Sedlák, Jaromír Kopeček, Vít Kopeckỳ, and Michal Landa. Resonant ultrasound spectroscopy–a tool to probe magneto-elastic properties of ferromagnetic shape memory alloys. *The European Physical Journal B*, 86(2):1–5, 2013.

[13] WP Mason. Piezoelectric crystals and their applications to ultrasonics, s. 427, 1950.

[14] Philip Shien Spoor. *Elastic properties of novel materials using PVDF film and resonant acoustic spectroscopy*. The Pennsylvania State University, 1996.

[15] Rohn Truell, Charles Elbaum, and Bruce B Chick. *Ultrasonic methods in solid state physics*. Academic press, 2013.

[16] Joseph Rhea Gladden III. *Characterization of the thin films and novel materials using resonant ultrasound spectroscopy*. The Pennsylvania State University, 2003.

[17] Augustus Edward Hough Love. *A treatise on the mathematical theory of elasticity*. Cambridge university press, 2013.

[18] RD Mindlin. Simple modes of vibration of crystals. *Journal of Applied Physics*, 27(12):1462–1466, 1956.

[19] Richard Holland. Resonant properties of piezoelectric ceramic rectangular parallelepipeds. *The Journal of the Acoustical Society of America*, 43(5):988–997, 1968.

[20] Ichiro Ohno. Free vibration of a rectangular parallelepiped crystal and its application to determination of elastic constants of orthorhombic crystals. *Journal of Physics of the Earth*, 24(4):355–379, 1976.

[21] William M Visscher, Albert Migliori, Thomas M Bell, and Robert A Reinert. On the normal modes of free vibration of inhomogeneous and anisotropic elastic objects. *The Journal of the Acoustical Society of America*, 90(4):2154–2162, 1991.

[22] Rasheed Adebisi. High temperature and pressure resonant ultrasound spectroscopy study of metal hydride systems. 2011.

[23] Brian J Zadler, Jérôme HL Le Rousseau, and Paul Freeman. Resonant ultrasound spectroscopy analysis codes. `https://github.com/PALab/RUS`.

[24] Brian J Zadler, Jérôme HL Le Rousseau, John A Scales, and Martin L Smith. Resonant ultrasound spectroscopy: theory and application. *Geophysical Journal International*, 156(1):154–169, 2004.

[25] Dynamic resonance systems, inc.

[26] Quasar pcri.

[27] Roditi, piezoelectric transducer crystals. `http://www.roditi.com/Transducer/Transducer-Crystals.html`.

[28] Boston piezo-optics inc. https://www.bostonpiezooptics.com/lithium-niobate.

[29] Shivprasad Patil, George Matei, Hang Dong, Peter M Hoffmann, Mustafa Karaköse, and Ahmet Oral. A highly sensitive atomic force microscope for linear measurements of molecular forces in liquids. *Review of Scientific Instruments*, 76(10):103705, 2005.

[30] Vojko matko and miro milanovic. https://doi.org/10.3390/s20030802.

[31] American piezo (apc) international ltd. https://www.americanpiezo.com/knowledge-center/piezo-theory/determining-resonance-frequency.html.

[32] Yasuhiro Ono, Tomoyuki Hikita, and Takuro Ikeda. Phase transitions in mixed crystal system k1-x (nh4) x h2po4. *Journal of the Physical Society of Japan*, 56(2):577–588, 1987.

[33] T Fukami. Refinement of the crystal structure of kh2po4 in the ferroelectric phase. *physica status solidi (a)*, 117(2):K93–K96, 1990.

[34] Cun Zhou, Fei Sun, and Xuzhao Liu. The effect factors of potassium dihydrogen phosphate crystallization in aqueous solution. In *AIP Conference Proceedings*, volume 1794, page 020003. AIP Publishing LLC, 2017.

[35] P Rajesh, P Ramasamy, and G Bhagavannarayana. Growth of adp–kdp mixed crystal and its optical, mechanical, dielectric, piezoelectric and laser damage threshold studies. *Journal of crystal growth*, 362:338–342, 2013.

[36] RFS Hearmon. The elastic constants of piezoelectric crystals. *British Journal of Applied Physics*, 3(4):120, 1952.

Appendix

1 Sample holder

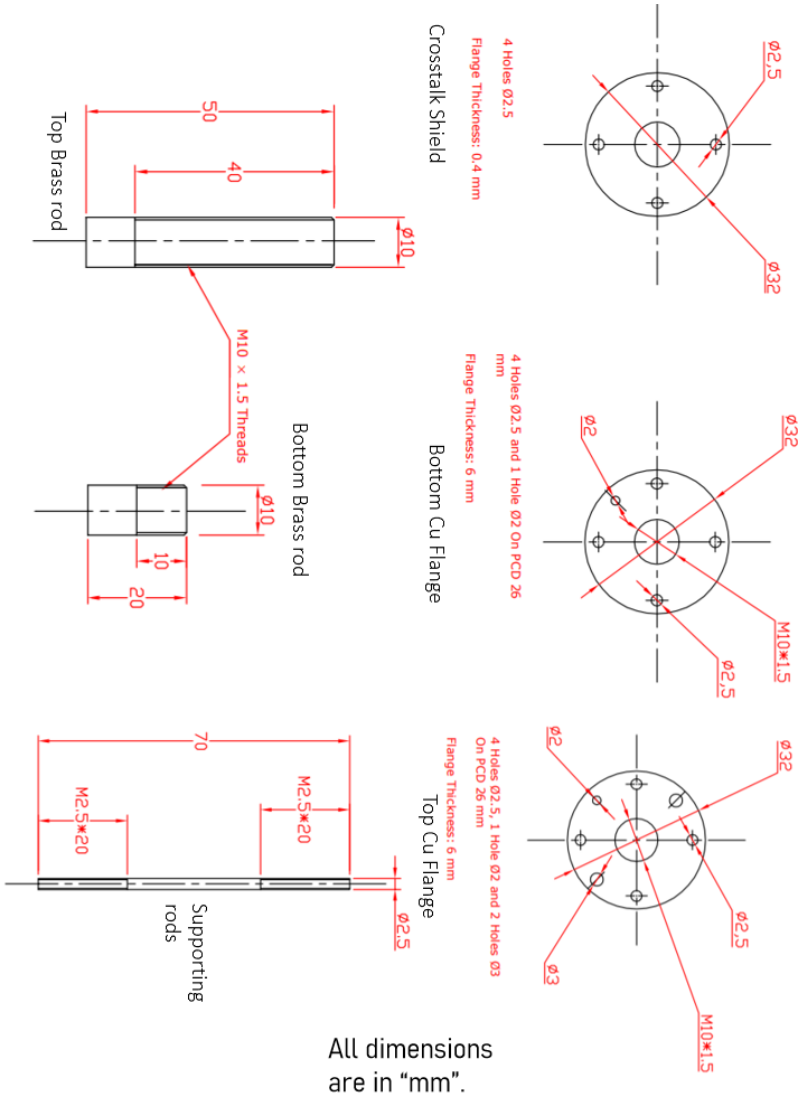

Sample Holder construction details: Copper flanges have disticntive four holes for supporting rods to pass through. Also, in the central hole of each flanges, the brass rods will pass. Notice that the bottom brass rod is shorter than the top brass rod. All of these components are put together by using the threadings made.

2 Data Acquisition LabView code

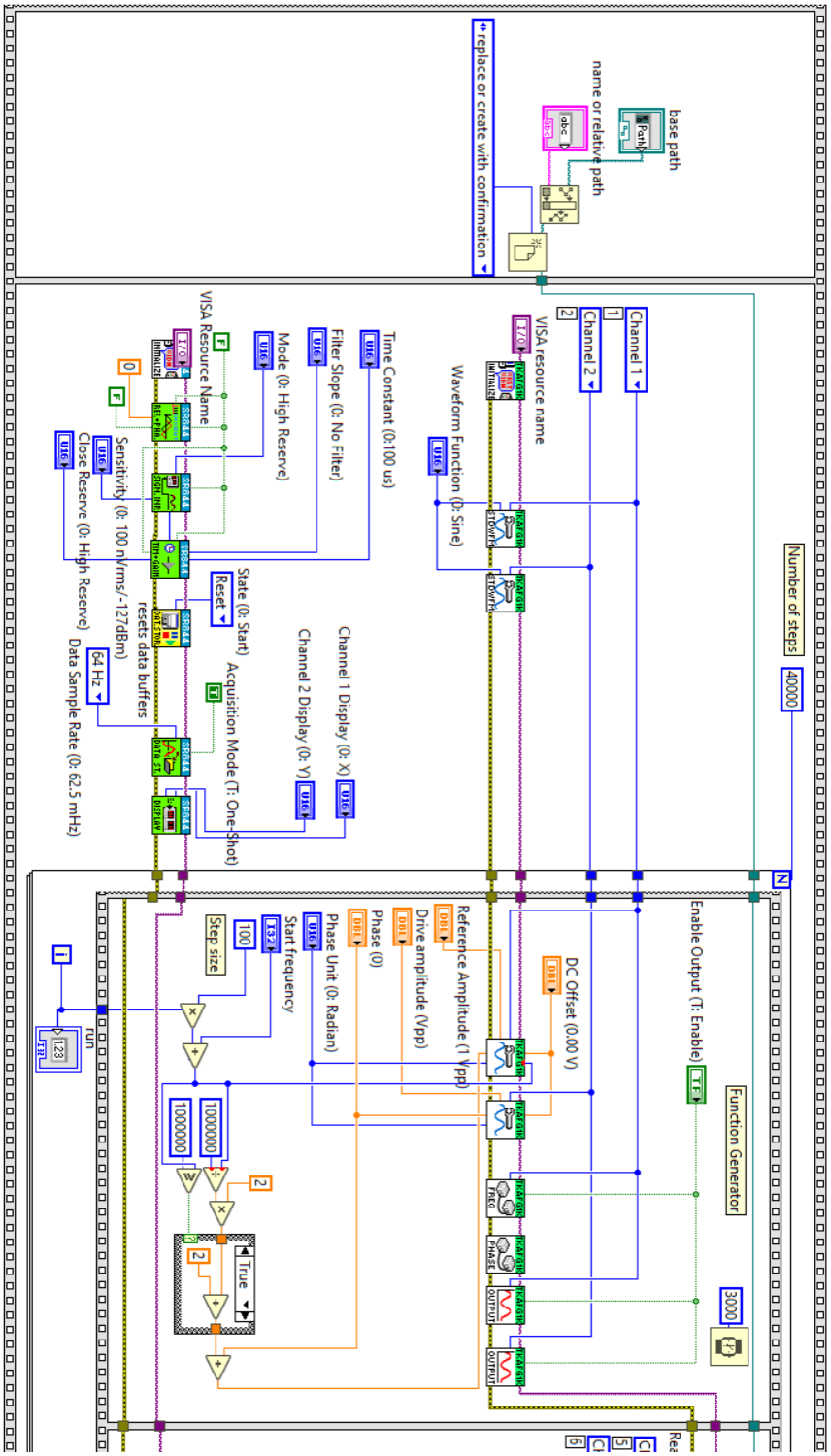

Data Acquisition code1

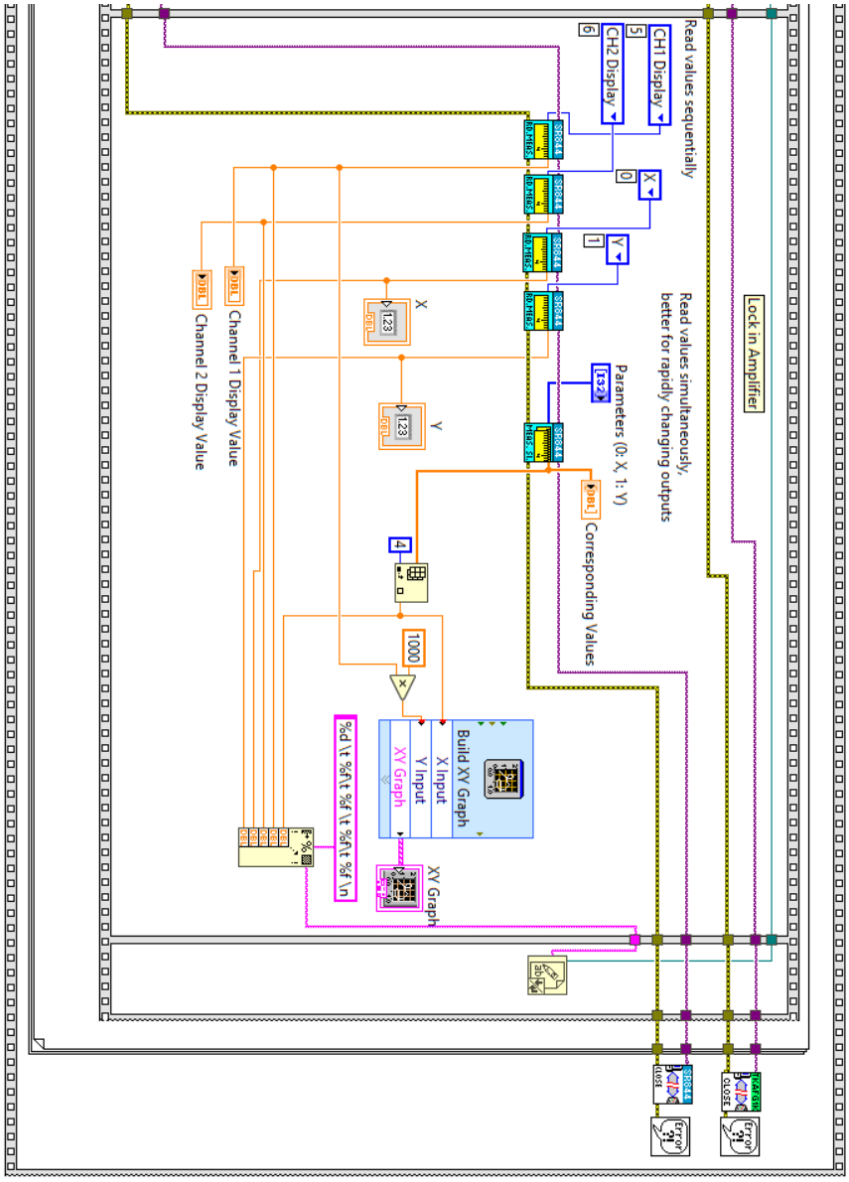

Data Acquisition code2

The instrumental VIs found on NI website are used to write this program. Using "flat sequence", the tasks of setting frequency on function generator and measuring signal on LIA are accomplished sequentially. And to run a full scan, a for loop is put over the flat sequence. Some configurations of the instruments are made before the for loop to avoid unneccesary repetitive settings.

3 Matlab Analysis codes

(a)

```
A=Frequency
B=detrend(Yo)% Y from scan 1
C=detrend(Yn)% Y from scan 2
D=detrend(Ym)% Y from scan 3
d=size(A);
e=d(1);
X=7000;% data pointsof Frequency per plot
for f=1:(e/X)
    %in each plot, specific patch of data points are selected.
    f
    K=A((X*(f-1)+1):(X*f),1);
    G=B((X*(f-1)+1):(X*f),1);
    Q=C((X*(f-1)+1):(X*f),1);
    R=D((X*(f-1)+1):(X*f),1);
    figure(f)
    set(gca,'FontSize',50)
    set(gcf, 'Position', [100,100,5000,3000])
    plot(K,G,"r-", "LineWidth", 2)
    [W,J]=max(G);%setting y axis limits
    [w,j]=min(G);
    avg=(W+w)/2;
    s=(W-w);
    ylim([avg-s,avg+s])
    hold on
    plot(K,Q,"b-", "LineWidth", 2)
    [M,I]=max(Q);
    [m,i]=min(Q);
    avg=(M+m)/2;
    p=(M-m);
    ylim([avg-p, avg+p])
    hold on
    plot(K,R,"cy-", "LineWidth", 2)
    [Z,Y]=max(R);
    [z,y]=min(R);
    avg=(Z+z)/2;
    q=(Z-z);
    ylim([avg-q,avg+q])
    xlabel("Frequency (in Hz)", "FontSize", 20)%labels
    ylabel("Quadrature (in V)", "FontSize", 20)
    legend('sample 3','sample 2','sample 1', "FontSize", 20)%legend
    hold off
    xlim([K(1),K(X)])
    %xlim([299041 498942])% limits to view only a particular freq. range
    %ylim([-0.0000795 0.0000690])
grid on
end
```

Code for comparing three Quadratures, used for plotting Fig. 4.2

(b)

```
A=Frequency
B=detrend(Yo)% Y from scan 1
C=detrend(Yn)% Y from scan 2
d=size(A);
e=d(1);
X=10000;% data pointsof Frequency per plot
T=TrueF % predicted frequencies from Forward code
for f=1:(e/X)
    %in each plot, specific patch of data points are selected.
    f
    K=A((X*(f-1)+1):(X*f),1);
    G=B((X*(f-1)+1):(X*f),1);
    Q=C((X*(f-1)+1):(X*f),1);

    figure(f)
    set(gcf, 'Position', [200,200,6000,3000])
    plot(K,G,"r-","LineWidth", 2)
    [W,J]=max(G);%setting y axis limits
    [w,j]=min(G);
    avg=(W+w)/2;
    s=(W-w)*0.2;
    ylim([avg-s,avg+s])
    hold on
    plot(K,Q,"b-", "LineWidth", 2)
    [M,I]=max(Q);
    [m,i]=min(Q);
    avg=(M+m)/2;
    p=(M-m)*0.2;
    ylim([avg-p,avg+p])
    hold on
       for freq=1:(100*f)
           h=0;
           if (T(freq)>(K(1)) && (T(freq)<K(X)))
               wq=T(freq)
           end
         plot(wq,h,'g*','LineWidth', 6)
           hold on
       end
    xlabel("Frequency (in Hz)","FontSize", 20)
    ylabel("Quadrature (in V)","FontSize", 20)
    legend('edge scan 1','edge scan 2','predicted',"FontSize", 20)
    hold off
    xlim([K(1),K(X)])
    grid on
end
```

Code for plotting predicted frequencies and experimentally observed peaks, used for plotting Fig. 4.2